Yamashita et al.

Figure 2. A, immunofluorescence analysis of gp130 and OSMR expression in HuH1 and HuH7 cell lines. B, immunofluorescence analysis of phosphorylated STAT3 expression in HuH1 and HuH7 cell lines stimulated by OSM (100 ng/mL for 1 hour) and controls. C, Western blotting analysis of whole or phosphorylated STAT3 protein expression in HuH1 and HuH7 cells stimulated by OSM (100 ng/mL for 1 hour) and controls. D, FACS analysis of HuH1 and HuH7 cells stained with FITC-conjugated anti-EpCAM antibodies. Top, EpCAM-high (designated as EpCAM[+]; yellow) and EpCAM-low/negative cells (designated as EpCAM[−]; blue) were enriched by magnetic activated cell sorting and labeled with FITC-conjugated anti-EpCAM antibodies or isotype control antibodies. Bottom, cells were cultured in 1% FBS DMEM with (green) or without OSM (100 ng/mL; orange) for 3 days and stained with FITC-conjugated anti-EpCAM antibodies.

—562—

alone could diminish EpCAM$^-$ non-CSCs which results in the enrichment of EpCAM$^+$ CSCs in HCC (18). We therefore explored the effect of 5-FU in combination with OSM on EpCAM$^+$ HCC cell proliferation and apoptosis *in vitro*.

When HuH1 and HuH7 cells were treated with OSM alone and cultured for 7 days, cell proliferation was modestly increased compared with untreated controls (Fig. 4A). In contrast, 5-FU treatment clearly inhibited cell proliferation.
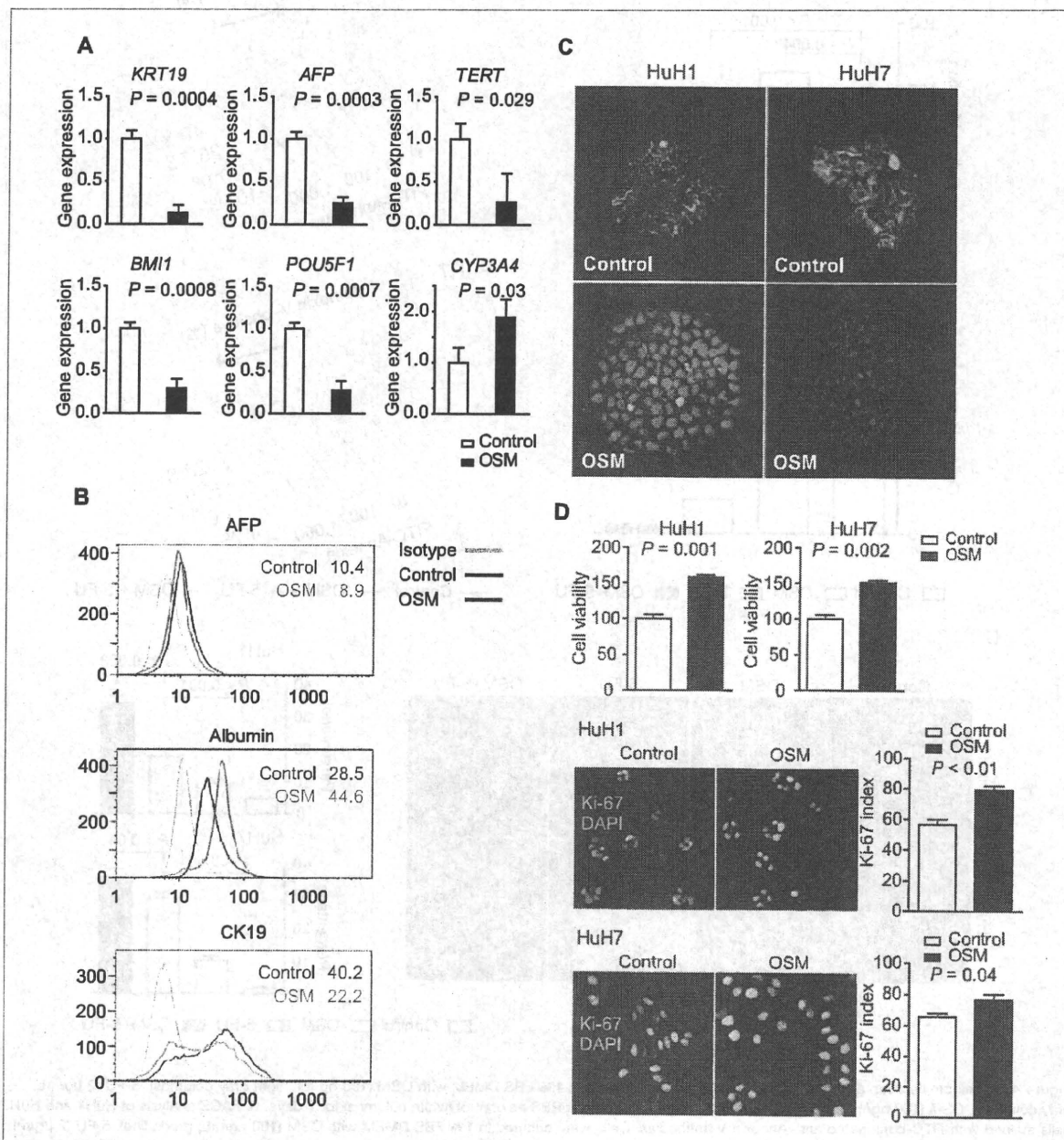

Figure 3. A, quantitative reverse transcription-PCR analysis of HuH1 cells cultured in 1% FBS DMEM with (black columns) or without (white columns) OSM (100 ng/mL) for 3 days. B, intracellular FACS analysis of HuH1 cells cultured in 1% FBS DMEM with (green line) or without (red line) OSM (100 ng/mL) for 3 days. The number in the figure indicates the geometric mean of the fluorescence intensity on a logarithmic scale. C, immunofluorescence analysis of HuH1 and HuH7 cell colonies cultured in 1% FBS DMEM with or without OSM (100 ng/mL) for 10 days. Colonies were fixed with 100% ice-cold methanol and stained with FITC-conjugated anti-EpCAM antibodies. D, top, cell proliferation assay of HuH1 and HuH7 cells cultured in 1% FBS DMEM with (black column) or without (white column) OSM (100 ng/mL) for 3 days. Middle and bottom, immunofluorescence analysis of HuH1 and HuH7 cells cultured in 1% FBS DMEM with or without OSM (100 ng/mL) for 3 days. Cells were fixed with 100% ice-cold methanol and stained with anti–Ki-67 antibodies.
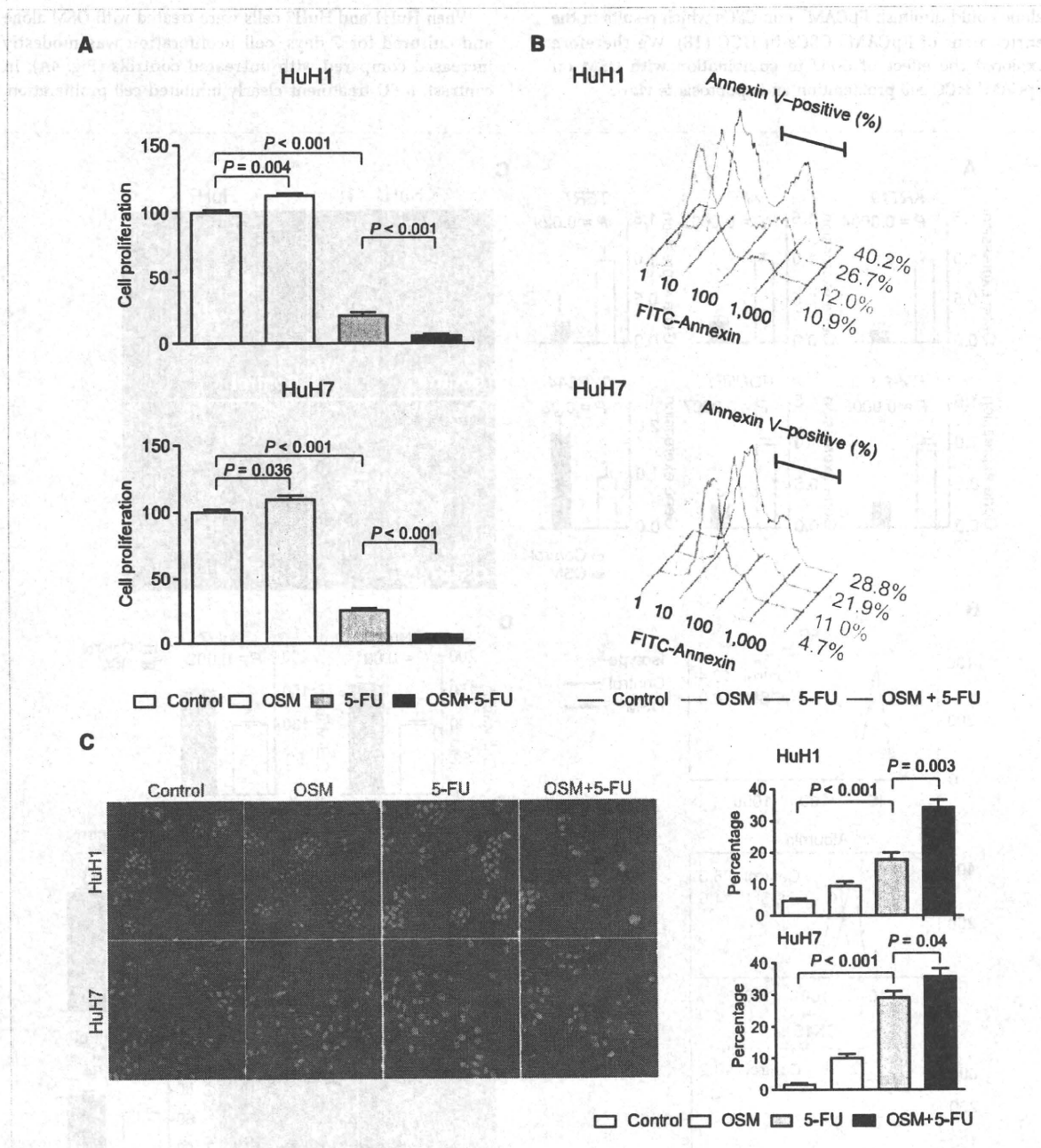
—563—

Figure 4. A, cell proliferation assay of HuH1 and HuH7 cells cultured in 1% FBS DMEM with OSM (100 ng/mL; light gray columns), 5-FU (2 µg/mL; gray columns), OSM (100 ng/mL) and 5-FU (2 µg/mL; black columns), or PBS as control (white columns) for 7 days. B, FACS analysis of HuH1 and HuH7 cells stained with FITC-conjugated anti–Annexin V antibodies. Cells were cultured in 1% FBS DMEM with OSM (100 ng/mL; green line), 5-FU (2 µg/mL; blue line), OSM (100 ng/mL) and 5-FU (2 µg/mL; red line), or PBS as control (gray line) for 3 days. C, left, immunofluorescence analysis of HuH1 and HuH7 cells stained with anti–active caspase 3 antibodies. Cells were cultured in 1% FBS DMEM with OSM (100 ng/mL), 5-FU (2 µg/mL), OSM (100 ng/mL) and 5-FU (2 µg/mL), or PBS control for 3 days. Right, bar graphs indicating the percentages of active caspase 3–positive cells.

Noticeably, the combination of OSM and 5-FU effectively suppressed cell proliferation in HuH1 and HuH7 cells (Fig. 4A). We further investigated the effects of OSM and 5-FU on apoptosis, evaluated by Annexin V binding to cell membranes and the activation of caspase 3 (Fig. 4B and C). Although OSM treatment alone had a small effect on the induction of apoptosis, 5-FU treatment induced Annexin V$^+$ and activated caspase 3$^+$ cells more than in the control. The

—564—

high serum AFP, frequent EpCAM positivity, and poorly differentiated morphology, suggesting that OSMR is more likely expressed in HCC with stem/progenitor cell features (16). Although the regulatory mechanisms of OSMR are still unclear, it is plausible that OSMR expression is regulated by a signaling pathway activated during the process of hepatogenesis. Because gp130 is known to be ubiquitously expressed, regulation of OSM signaling might be largely dependent on the expression status of OSMR in normal and tumor tissues. Recent studies have shown the potential role of methylation of CpG islands located in OSMR promoter in colorectal cancer (31, 32). Clarification of OSMR promoter activity regulation, including CpG methylation, might provide clues for better understanding of hepatocytic differentiation signaling in both normal hepatic stem cells and CSCs.

It has been postulated that both normal stem cells and CSCs are dormant and show slow cell cycles. Consistent with this, CSCs are considered to be more resistant to chemotherapeutic agents than non-CSCs, possibly due to slow cell cycles as well as an increased expression of ATP-binding cassette transporters, robust DNA damage responses, and activated antiapoptotic signaling (20, 33, 34). Therefore, development of an effective strategy by targeting CSC pools together with conventional chemotherapies is essential to eradicate a tumor mass. Two strategies have been investigated to reduce the CSCs population in the tumor; that is, inhibition of self-renewal programs and activation of differentiation programs. We have shown that hepatocytic differentiation of liver CSCs by OSM results in enhanced cell proliferation *in vitro*. We have further shown here that OSM-mediated hepatocytic differentiation of liver CSCs in combination with conventional chemotherapy effectively suppresses HCC growth. It is possible that OSM may boost antitumor activity of 5-FU by "exhausting dormant CSCs" through hepatocytic differentiation and active cell division. It is encouraging that similar success with differentiation therapy has recently been reported in several cancers (24, 35, 36). In addition, HNF4-α–mediated differentiation of HCC cells has recently been reported to be effective for the eradication of HCC (37). However, although the combination of OSM and 5-FU effectively inhibited tumor growth in our model, we could not observe the shrinkage of the tumor. Thus, induction of CSC's differentiation with eradication of non-CSCs might not be enough for the eradication of the tumor, which might suggest the importance of inhibiting self-renewal as well as stimulating differentiation of CSCs. Because we induced the hepatocytic differentiation of the subcutaneous tumor by local injection of OSM, further rigorous studies are clearly required to assess the effect of OSM on liver CSCs and its utility for differentiation therapy in HCC.

CSCs may acquire resistance against differentiation therapy by additional genetic/epigenetic changes during treatment by clonal evolution, as observed in conventional chemotherapy. Indeed, it has recently been suggested that bone morphogenetic protein–mediated brain CSC differentiation failed in a subset of brain tumors in which bone morphogenetic protein receptor promoters were methylated and silenced (23). Similarly, OSMR silencing by promoter methylation might result in the development of OSM-resistant clones in HCC.

In conclusion, OSMR is expressed in certain types of HCC with stem/progenitor cell features, and OSM induces hepatocytic differentiation and active cell division of OSMR$^+$ liver CSCs to enhance chemosensitivity to 5-FU. The clinical safety and utility of OSM should be evaluated in the near future.

Disclosure of Potential Conflicts of Interest

Acknowledgments

Grant Support

References

1. Fialkow PJ. Clonal origin of human tumors. Biochim Biophys Acta 1976;458:283–321.
2. Clarke MF, Dick JE, Dirks PB, et al. Cancer stem cells—perspectives on current status and future directions: AACR Workshop on Cancer Stem Cells. Cancer Res 2006;66:9339–44.
3. Jordan CT, Guzman ML, Noble M. Cancer stem cells. N Engl J Med 2006;355:1253–61.
4. Al-Hajj M, Wicha MS, Benito-Hernandez A, Morrison SJ, Clarke MF. Prospective identification of tumorigenic breast cancer cells. Proc Natl Acad Sci U S A 2003;100:3983–8.
5. Bonnet D, Dick JE. Human acute myeloid leukemia is organized as a hierarchy that originates from a primitive hematopoietic cell. Nat Med 1997;3:730–7.
6. O'Brien CA, Pollett A, Gallinger S, Dick JE. A human colon cancer cell capable of initiating tumour growth in immunodeficient mice. Nature 2007;445:106–10.
7. Ricci-Vitiani L, Lombardi DG, Pilozzi E, et al. Identification and expansion of human colon-cancer-initiating cells. Nature 2007; 445:111–5.
8. Singh SK, Hawkins C, Clarke ID, et al. Identification of human brain tumour initiating cells. Nature 2004;432:396–401.
9. Visvader JE, Lindeman GJ. Cancer stem cells in solid tumours: accumulating evidence and unresolved questions. Nat Rev Cancer 2008;8:755–68.
10. El-Serag HB, Rudolph KL. Hepatocellular carcinoma: epidemiology and molecular carcinogenesis. Gastroenterology 2007;132: 2557–76.
11. Mishra L, Banker T, Murray J, et al. Liver stem cells and hepatocellular carcinoma. Hepatology 2009;49:318–29.
12. Chiba T, Kita K, Zheng YW, et al. Side population purified from hepatocellular carcinoma cells harbors cancer stem cell-like properties. Hepatology 2006;44:240–51.

combination of OSM and 5-FU most strongly induced apoptosis in both HuH1 and HuH7 cells with statistical significance.

Finally, we investigated the effect of OSM on EpCAM⁺ HCC *in vivo* using a primary HCC specimen and cell lines. Single-cell suspensions from primary EpCAM⁺ HCC cells (1×10^6 cells) were injected into 6-week-old male NOD/SCID mice, and these cells formed subcutaneous tumors 48 days after transplantation. Subsequently, 50 μL of PBS, OSM (2 μg/tumor), 5-FU (250 μg/tumor), or OSM (2 μg/tumor) and 5-FU (250 μg/tumor) solution were injected directly into each tumor twice a week. Although OSM treatment alone showed weak tumor-suppressive effects, the changes in tumor size showed no significant difference compared with controls (Fig. 5A). Similarly, 5-FU treatment alone showed limited tumor-suppressive effects. However, the combination of OSM with 5-FU showed a marked inhibition of tumor growth compared with PBS control or 5-FU alone ($P = 0.02$ and 0.05, respectively). Immunohistochemical analysis of xenografted tumors showed that OSM treatment decreased the number of EpCAM⁺ or CK19⁺ cells and increased CYP3A4⁺ cells *in vivo* (Supplementary Fig. S3A and B). FACS analysis of xenografted tumors further confirmed the decrease of EpCAM⁺ cell population by OSM treatment *in vivo* (Supplementary Fig. S3C). Immunohistochemical analysis revealed that the combination of OSM with 5-FU strongly induced the activation of caspase 3 compared with PBS control, OSM, or 5-FU (Fig. 5B). Taken together, these data suggest that hepatocytic differentiation of EpCAM⁺ HCC cells induced by OSM was the most effective for inhibition of tumor growth *in vivo* when the conventional chemotherapeutic agent 5-FU was coadministered.

Discussion

A growing body of evidence suggests that there are similarities between normal stem cells and CSCs in terms of self-renewal programs (29). We have recently reported that Wnt/β-catenin signaling augments self-renewal and inhibits the differentiation of EpCAM⁺ liver CSCs (18). In the present study, we have shown that the OSM-OSMR signaling pathway is maintained in HCCs with stem/progenitor cell features. OSM induces hepatocytic differentiation and activates cell division in dormant EpCAM⁺ liver CSCs (Fig. 5C). Furthermore, we have shown that the combination of OSM and 5-FU effectively inhibits tumor cell growth, revealing the importance of targeting both CSCs and non-CSCs for eradication of the tumor.

OSM is a pleiotropic cytokine that belongs to the IL-6 family which includes IL-6, IL-11, and leukemia-inhibitory factor. These cytokines share the gp130 receptor subunit as a common signal transducer, and activate Janus tyrosine kinases and the STAT3 pathway. However, gp130 forms a heterodimer with a unique partner such as the IL-6 receptor, leukemia-inhibitory factor receptor, or OSMR, thus transducing a certain signaling uniquely induced by each cytokine (30). Of note, OSM is known to activate hepatocytic differentiation programs in hepatoblasts in an OSMR-specific manner (27), and our data showed that OSM could induce

hepatocytic differentiation and active cell proliferation in EpCAM⁺ HCC through OSMR signaling.

OSMR is expressed in hepatoblasts in the fetal liver (26). We have found that OSMR is frequently expressed in normal hepatic progenitors but is rarely detected in hepatocytes in adult livers. Interestingly, OSMR⁺ HCC was characterized by
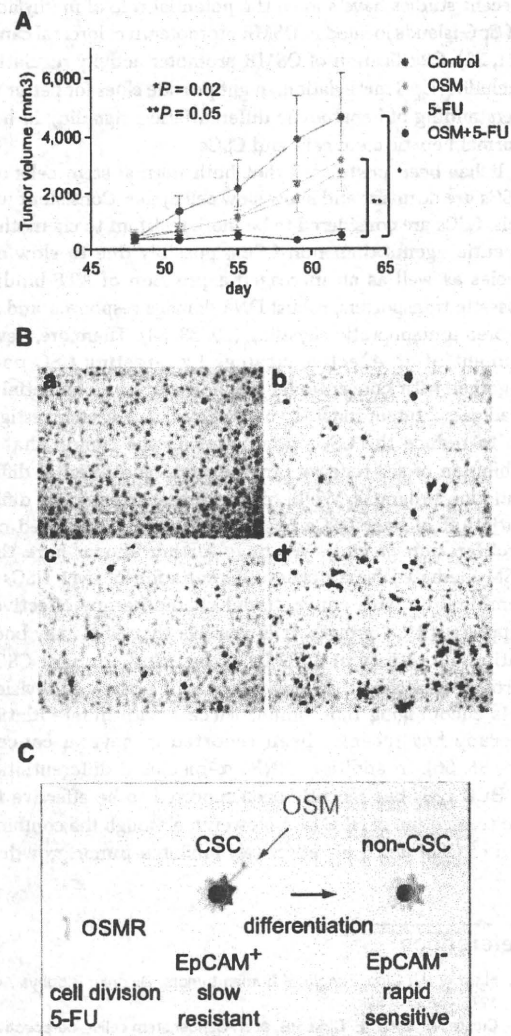

Figure 5. A, effect of PBS, OSM, 5-FU, and OSM plus 5-FU injections on the growth of primary EpCAM⁺ AFP⁺ HCC xenograft tumors in NOD/SCID mice (*n* = 4 in each group). Intratumoral injection of 50 μL of PBS, OSM (2 μg/tumor), 5-FU (250 μg/tumor), or OSM (2 μg/tumor) and 5-FU (250 μg/tumor) was initiated 48 days after transplantation, twice per week. B, representative images of activated caspase 3 staining of xenograft tumors in each treatment group (a, PBS; b, OSM; c, 5-FU; and d, OSM and 5-FU). C, a schematic diagram of the effect of OSM on EpCAM⁺ liver CSCs. Dormant EpCAM⁺ liver CSCs with OSMR expression respond to OSM and differentiate into rapidly dividing EpCAM⁻ non-CSCs that are highly sensitive to 5-FU.

—566—

ORIGINAL ARTICLE

Accelerated hepatocellular carcinoma development in mice expressing the *Pim-3* transgene selectively in the liver

Y Wu[1,2], YY Wang[2], Y Nakamoto[3], Y-Y Li[2,4], T Baba[2], S Kaneko[3], C Fujii[2,5] and N Mukaida[2]

[1]Department of Hematology and Hematology research Laboratory, State Key Laboratory of Biotherapy and Cancer Center, West China Hospital, Sichuan University, Chengdu, Sichuan Province, PR China; [2]Division of Molecular Bioregulation, Cancer Research Institute, Kanazawa University, 13-1 Takara-machi, Kanazawa, Japan; [3]Department of Disease Control and Homeostasis, Graduate School of Medical Sciences, Kanazawa University, 13-1 Takara-machi, Kanazawa, Japan and [4]Researcher Center, Fudan University Cancer Hospital, Shanghai, PR China

Pim-3, a proto-oncogene with serine/threonine kinase activity, was enhanced in hepatocellular carcinoma (HCC) tissues. To address the roles of Pim-3 in HCC development, we prepared transgenic mice that express human Pim-3 selectively in liver. The mice were born at a Mendelian ratio, were fertile and did not exhibit any apparent pathological changes in the liver until 1 year after birth. Pim-3-transgenic mouse-derived hepatocytes exhibited accelerated cell cycle progression. The administration of a potent hepatocarcinogen, diethylnitrosamine (DEN), induced accelerated proliferation of liver cells in Pim-3 transgenic mice in the early phase, compared with that observed for wild-type mice. Treatment with DEN induced lipid droplet accumulation with increased proliferating cell numbers 6 months after the treatment. Eventually, wild-type mice developed HCC with a frequency of 40% until 10 month after the treatment. Lipid accumulation was accelerated in Pim-3 transgenic mice with higher proliferating cell numbers, compared with that observed for wild-type mice. Pim-3 transgenic mice developed HCC with a higher incidence (80%) and a heavier burden, together with enhanced intratumoral CD31-positive vascular areas, compared with that observed for wild-type mice. These observations indicate that Pim-3 alone cannot cause, but can accelerate HCC development when induced by a hepatocarcinogen, such as DEN.

Correspondence: Dr N Mukaida, Division of Molecular Bioregulation, Cancer Research Institute, Kanazawa University, 13-1 Takara-machi, Kanazawa, Ishikawa 920-0934, Japan.
E-mail: naofumim@kenroku.kanazawa-u.ac.jp
[5]Present address, Department of Integrative Physiology, School of Medicine, Shinshu University, 3-1-1 Asahi, Matsumoto 390-8621, Japan.

Introduction

There were over 667000 new cases of hepatocellular carcinoma (HCC) worldwide in 2005. The 5-year survival rate of individuals with hepatic malignancy is only 8.9% despite aggressive conventional therapy, making hepatic malignancy the second most lethal cancer among human malignancies (Farazi and DePinho, 2006; Umemura et al., 2009). Hepatocellular carcinoma usually arises in conditions that can cause liver cirrhosis, such as chronic hepatitis B and C viral infection, chronic alcohol consumption and intake of food contaminated with aflatoxin-B_1 (Zheng et al., 2007). These conditions generally provoke continuous rounds of hepatocyte damage in the setting of chronic hepatitis or liver cirrhosis, and eventually activate resident or inflammatory non-parenchymal cells to produce growth factors and cytokines (Otani et al., 2005). The produced factors can drive compensatory and aberrant proliferation of surviving hepatocytes and development of pre-malignant dysplastic nodules that form the nucleus of neoplastic lesions. Only recently has the molecular analysis of human HCC unraveled many genetic and epigenetic alterations that result in the deregulation of key proto-oncogenes and tumor-suppressor genes, including TP53, β-catenin, ErbB receptors family members, *met* and its ligand, hepatocyte growth factor, p16, E-cadherin and cyclo-oxygenase 2 (Hosono et al., 1993). However, roles of other proto-oncogenes and tumor suppressor genes in HCC development still remain elusive (Thorgeirsson and Grisham, 2002).

We previously identified *Pim-3*, a proto-oncogene with serine/threonine kinase activity, as the gene selectively expressed in pre-malignant and malignant lesions of the mouse HCC model in transgenic mice expressing hepatitis B virus surface antigen (Fujii et al., 2005). *Pim-3* was originally identified as a depolarization-induced gene, *KID-1*, in PC12 cells, a rat pheochromocytoma cell line (Feldman et al., 1998). Subsequently, Deneen et al. (2003) demonstrated that *Pim-3* gene transcription was enhanced in the EWS/ETS-induced malignant transformation of NIH 3T3 cells, suggesting the involvement of Pim-3 in tumorigenesis. Consistently, we observed that Pim-3 expression was enhanced in

carcinomas but not in normal tissues of human endoderm-derived organs, including the liver (Fujii *et al.*, 2005), pancreas (Li *et al.*, 2006), colon (Popivanova *et al.*, 2007) and stomach (Zheng *et al.*, 2008). Moreover, Pim-3 can inactivate a pro-apoptotic molecule, Bad, and maintain the expression of an anti-apoptotic molecule, Bcl-X$_L$, and prevent apoptosis of human pancreatic cancer and colon cancer cells (Li *et al.*, 2006). Similarly, the ablation of endogenous Pim-3 by short interfering RNA reduced the cell growth of human HCC cell lines by inducing their apoptosis (Fujii *et al.*, 2005).

These observations prompted us to investigate the effects of liver-specific Pim-3 overexpression on HCC development. Although we could not observe spontaneous HCC development in liver-specific Pim-3 transgenic mice, these mice developed HCC with a higher incidence and a heavier hepatocarcinoma burden, when a potent hepatocarcinogen, diethylnitrosamine (DEN), was administered during the suckling period. These results suggest that Pim-3 can accelerate but is not likely the primary inducer of HCC development.

Results

Characterization of transgenic mice overexpressing Pim-3 under the control of the albumin promoter

Pim-3 transgenic mice were born at a Mendelian ratio, were fertile and did not show any apparent abnormalities in the liver until 1 year after birth (data not shown). We first examined the expression pattern of Pim-3 in Pim-3 transgenic mice. Mouse *Pim-3* messenger RNA (mRNA) was detected in liver at a similar extent in both wild-type (WT) and Pim-3 transgenic mice, whereas human *Pim-3* mRNA was exclusively detected in Pim-3 transgenic mice (Figure 1b). Consistently, Pim-3 protein

was detected abundantly in liver of Pim-3 transgenic mice but not WT mice (Figure 1b). Pim-3 protein was also detected in the heart and kidney of Pim-3 transgenic mice, but not of WT mice (Figure 1c). As anti-Pim-3 recognizes both human and mouse Pim-3 to a similar degree, we further examined the mRNA of human and mouse Pim-3 in the liver, heart and kidney. Human *Pim-3* mRNA was detected in the liver of Pim-3 transgenic mice, but not in other organs (Figure 1d). These observations would indicate that Pim-3 transgenic mice express human Pim-3 abundantly and selectively in liver.

Enhanced hepatocyte proliferation by Pim-3 overexpression

As Pim-3 can phosphorylate a pro-apoptotic molecule, Bad, at the Ser^{112} residue but not at the Ser^{136} residue, we first examined the phosphorylation states of Bad, to prove the functionality of the *Pim-3* gene, selectively overexpressed in liver. Bad was constitutively phosphorylated at Ser^{112} in hepatocytes from Pim-3 transgenic but not WT mice (Figure 2a). However, the level of phospho-Ser^{136}–Bad was not enhanced in Pim-3 transgenic mice. These observations would indicate that overexpressed Pim-3 was functional in terms of its capacity to phosphorylate Bad, its substrate. The levels of cyclin D1 and proliferating cell nuclear antigen (PCNA) in hepatocytes were increased in Pim-3 transgenic mice, compared with that observed for WT mice (Figure 2b). Moreover, cell cycle analysis of isolated heptocytes revealed that the proportion of the cells in subG1 phase, which represent apoptotic cells, was marginally but not significantly decreased in Pim-3 transgenic mice. However, the proportion of the cells in G2/M phase was significantly increased in Pim-3 transgenic mice compared with that observed for WT mice (Figure 2c). To exclude the possibility that
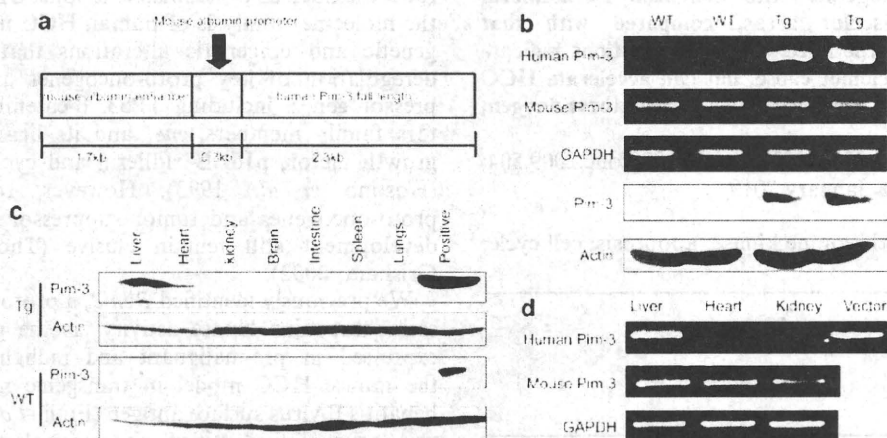
Figure 1 Expression of Pim-3 in alb-Pim-3 transgenic mice. (**a**) The schematic representation of the gene used for preparation of Pim-3 transgenic mice. (**b**) Expression of human (transgenic) and mouse (endogenous) *Pim-3* mRNA and protein levels in liver. The upper three lines are assessed by RT–PCR, whereas the lower two lines are assessed by immunoblotting. Representative results from five independent animals are shown here. (**c**) Immunoblotting analysis of Pim-3 protein expression in the liver, heart, kidney, brain, intestine, spleen and lungs of Pim-3 transgenic mice. The human embryonic kidney (HEK293) cells transfected with human Pim-3 complementary DNA (cDNA) were used as a positive control. Representative results from five independent animals are shown here. (**d**) Endogenous mouse *Pim-3* mRNA expression in the liver, heart and kidney of Pim-3 transgenic mice were determined by RT–PCR. Representative results from five independent animals are shown here.
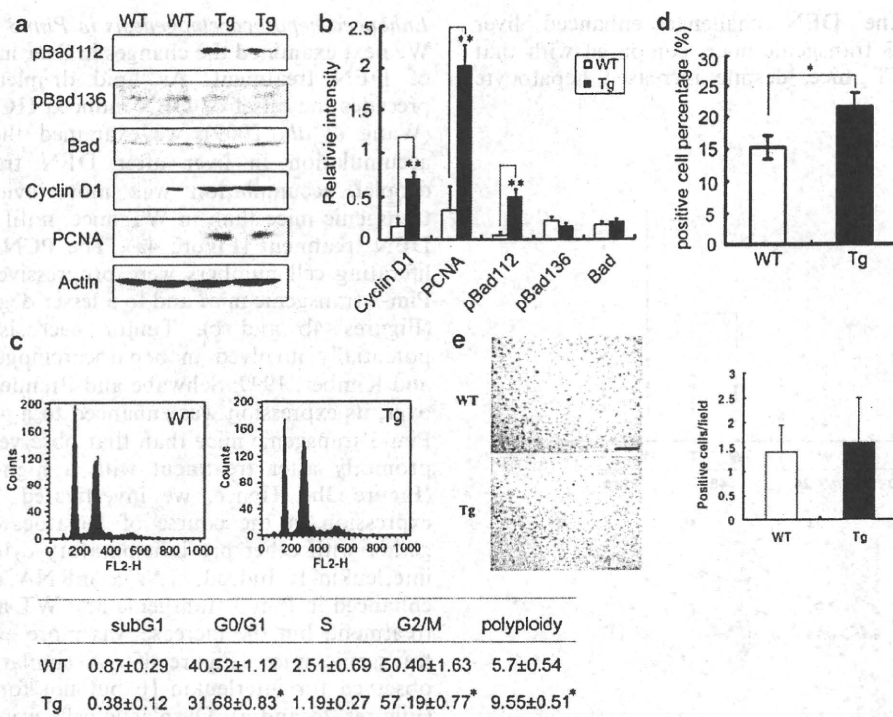
Figure 2 The effects of Pim-3 overexpression on hepatocyte functions. Hepatocytes were obtained from 3-week-old wild-type (WT) and Pim-3 transgenic (Tg) mice and used for the following analyses. (a and b) Protein was extracted from purified hepatocytes from WT and Tg mice, and was subjected to immunoblotting using anti-phospho-Ser^{112}-Bad, anti-phospho-Ser^{136}-Bad, anti-Bad, anti-cyclin D1 and anti-PCNA (proliferating cell nuclear antigen) antibodies as described in Materials and methods section. Representative results from four independent experiments are shown in (a). The intensity of each band was determined using National Institutes of Health (NIH) Image Analysis software version 1.62 (NIH, Bethesda, MD, USA), and its ratios to β-actin were calculated and are shown in (b) ($n = 4$). Open boxes, WT mice; closed boxes, Pim-3 Tg mice. ** $P < 0.01$. (c) DNA contents were determined for hepatocytes from WT and Pim-3 Tg mice as described in Materials and methods section. Representative results from five independent experiments are shown here. After the proportion of each fraction was determined, mean and 1 s.d. were calculated and are shown in the Table (inlet; $n = 5$). * $P < 0.05$; * $P < 0.01$. (d) The proportion of cyclin B1-positive cells was determined on liver tissues obtained from 3-week-old Pim-3 trangenic and WT mice as described in Materials and methods section. Mean and s.e.m. values were calculated ($n = 6$) and are shown here. (e) The terminal transferase dUTP nick end labeling (TUNEL) assay was conducted as described in Materials and methods section. Representative results from five individual animals are shown in the left panel. Positive cells were determined in five randomly chosen fields (× 400) from each animal by an examiner without any knowledge of experimental procedures. Mean ± s.d. values are shown in the right panel ($n = 5$).

isolation of hepatocytes from liver gave rise to artificially high proportion of cells in G2/M phase, we also enumerated the proportion of cells in G2/M phase by immunostaining liver tissues with anti-cyclin B1 antibodies. The proportion of cyclin B1-positive cells were significantly higher in Pim-3 transgenic mice than in WT mice (Figure 2d). Moreover, TUNEL (terminal transferase dUTP nick end labeling) staining failed to detect any significant differences in the numbers of apoptotic hepatocytes between untreated WT and Pim-3 transgenic mice (Figure 2e). These observations suggest that Pim-3 overexpressed in liver can accelerate the cell cycle progression of hepatocytes.
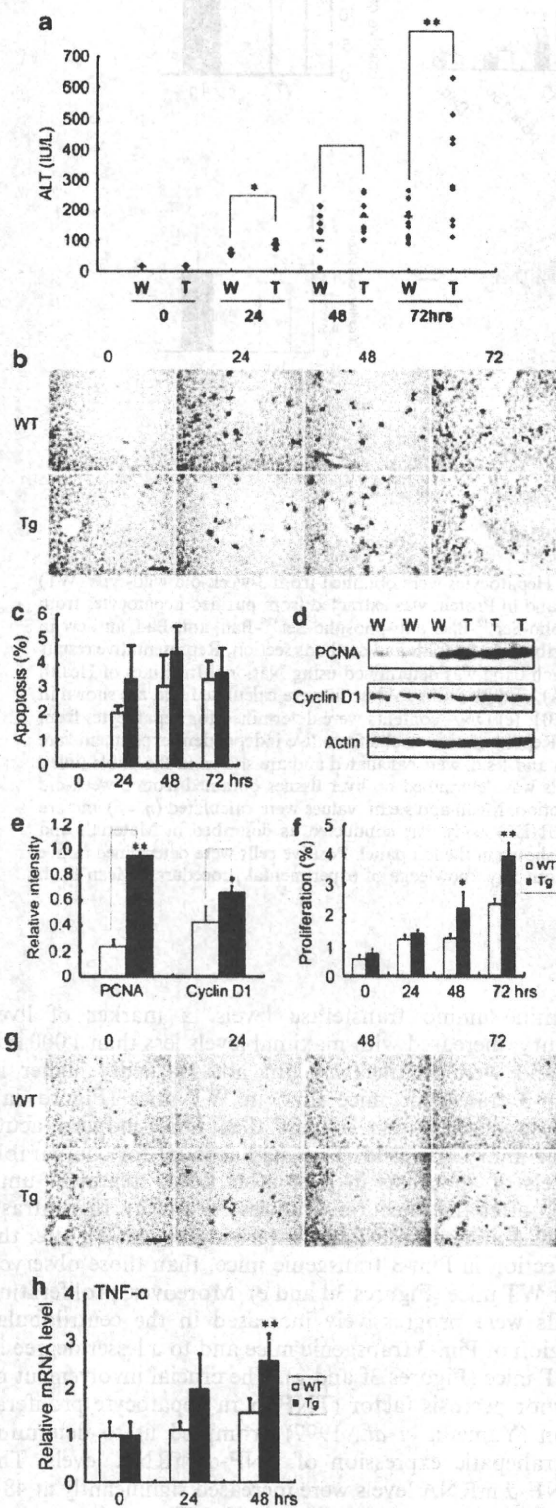
Enhanced liver damage in Pim-3 transgenic mice
We then treated Pim-3 transgenic and WT mice with DEN, a potent hepatocarcinogen. Both Pim-3 transgenic and WT mice survived exposure to DEN. Serum

alanine amino transferase levels, a marker of liver injury, increased with maximal levels less than 1 000 IU/ l, and were significantly but not markedly higher in Pim-3 transgenic mice than in WT mice (Figure 3a). These observations suggest that DEN-induced acute liver injury was mild. This may account for comparable levels of apoptosis in liver after DEN treatment until 72 h after the injection (Figures 3b and c). In contrast, PNCA and cyclin D1 levels were higher, at 72 h after the injection in Pim-3 transgenic mice, than those observed for WT mice (Figures 3d and e). Moreover, proliferating cells were progressively increased in the centrilobular region of Pim-3 transgenic mice and to a lesser degree in WT mice (Figures 3f and g). The crucial involvement of tumor necrosis factor (TNF)-α in hepatocyte proliferation (Yamada et al., 1997) prompted us to determine intrahepatic expression of TNF-α mRNA levels. The TNF-α mRNA levels were increased significantly at 48 h after DEN treatment (Figure 3h). These observations

indicate that the DEN challenge enhanced liver damage in Pim-3 transgenic mice, compared with that observed for WT mice, despite increased hepatocyte proliferation.

Enhanced hepatocarcinogenesis in Pim-3 transgenic mice
We next examined the changes in liver in the later phase of DEN treatment. As lipid droplet accumulation precedes the onset of DEN-induced HCC development (Wang *et al.*, 2009), we examined the lipid droplet accumulation in liver after DEN treatment. Lipid droplet accumulation was more evident in Pim-3 transgenic mice than in WT mice, until 6 months after DEN treatment (Figure 4a). The PCNA-positive proliferating cell numbers were progressively increased in Pim-3 transgenic mice and to a lesser degree in WT mice (Figures 4b and c). Tumor necrosis factor-α was potentially involved in hepatocarcinogenesis (Roberts and Kimber, 1999; Schwabe and Brenner, 2006). Moreover, its expression was enhanced to a greater extent in Pim-3 transgenic mice than that observed for WT mice promptly after treatment with a high-dose of DEN (Figure 3h). Hence, we investigated *TNF-α* mRNA expression in the course of hepatocarcinogenesis together with other pro-inflammatory cytokines, such as interleukin-1. Indeed, *TNF-α* mRNA expression was enhanced in Pim-3 transgenic and WT mice after DEN treatment, but the increase was more evident in Pim-3 transgenic mice (Figure 4f). A similar tendency was observed for interleukin-1β but not for interleukin-1α (Figures 4d and e). Dysplastic cells were observed and lobules were distorted in livers of Pim-3 transgenic mice, but not of WT mice, 6 months after DEN treatment (Figure 5a). At 10 months after the injection, nodules consisting of highly dysplastic malignant cells were observed in liver of Pim-3 transgenic mice and to a lesser extent in WT mice (Figure 5a). Macroscopically,

Figure 3 The effects of overexpressed Pim-3 on apoptosis and cell proliferation after diethylnitrosamine (DEN) treatment. (a) Serum alanine amino transferase (ALT) levels were determined as described in Materials and methods section. Each symbol indicates serum ALT level of each animal and the bars represent the median of each group. *P<0.05; **P<0.01 vs wild-type (WT) mice. (b and c) Liver tissues were obtained from WT or transgenic (Tg) mice at the indicated time intervals and immunostained with anti-cleaved caspase 3 antibody. Representative results from five independent animals are shown in (b) with an original magnification ×400. Proportion of cleaved caspase 3-positive apoptotic cells were determined as described in Materials and methods section. Mean±s.d. values are shown in (c) (n=5). Open boxes, WT mice; closed boxes, Pim-3 transgenic mice. (d and e) Cell lysates were obtained from liver of WT (W) and Pim-3 transgenic mice (T) at 72h after DEN treatment and subjected to immunoblotting using anti-PCNA (proliferating cell nuclear antigen) or anti-cyclin D1 antibodies. Representative results from three independent experiments are shown in (d). The intensity of each band was determined and its ratio to β-actin was calculated. Mean±s.d. values are shown in (e) (n=5). Open boxes, WT mice; closed boxes, Pim-3 transgenic mice. *P<0.05; **P<0.01 vs WT mice. (f and g) Liver tissues were obtained from WT or Tg mice at the indicated time intervals and immunostained with anti-PCNA antibody. Representative results from five independent animals are shown in (g) with an original magnification ×400. PCNA-positive proliferating cell numbers were determined as described in Materials and methods section. Mean±s.d. values are shown in (f) (n=5). *P<0.05; **P<0.01 vs WT mice. (h) Intrahepatic tumor necrosis factor-α (TNF-α) mRNA levels were determined as described in Materials and methods section. **P<0.01 vs WT mice (n=5).
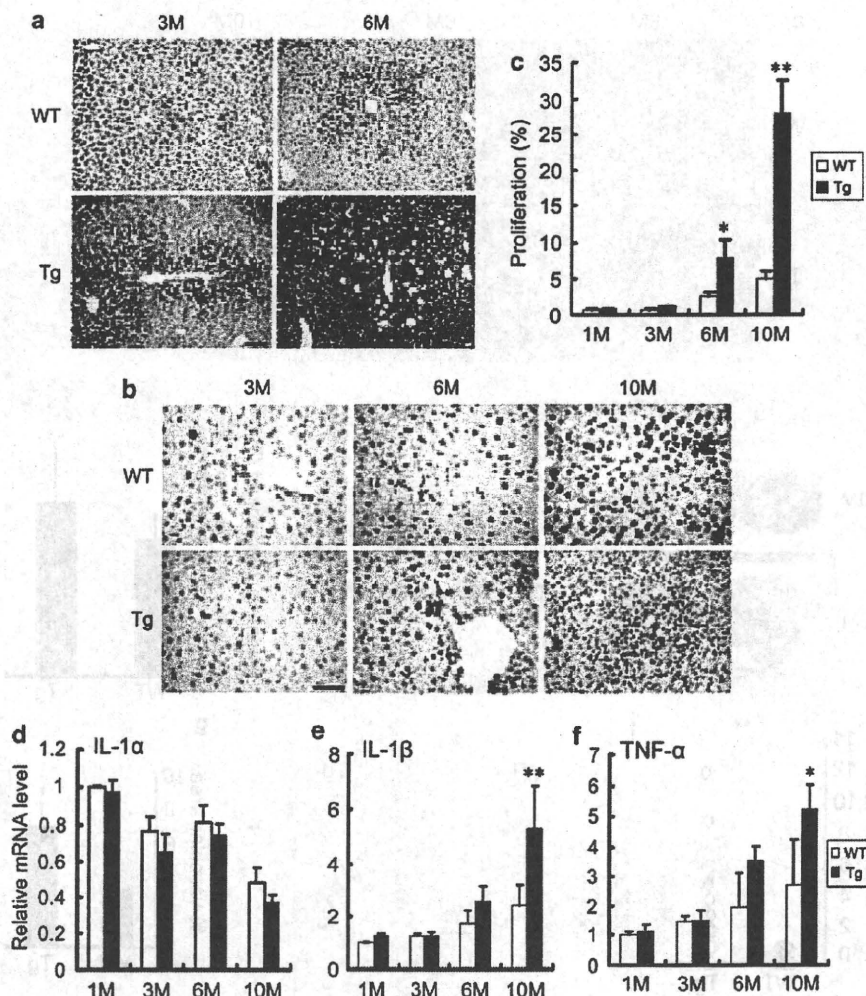
Figure 4 The effects of Pim-3 overexpression in liver pathology in the later phase after diethylnitrosamine (DEN) treatment. (a) The liver was obtained from wilt-type (WT) or Pim-3 transgenic mice (Tg) at the indicated time intervals and was subjected to staining with oil red solution as described in Materials and methods section. Representative results from five independent animals are shown with an original magnification × 200. (b and c) The livers were obtained from WT or Pim-3 Tg mice at the indicated time intervals and were subjected to immunostaining with anti-PCNA (proliferating cell nuclear antigen) antibody as described in Materials and methods section. Representative results from five independent animals are shown in (b) with an original magnification × 400. PCNA-positive cell numbers were determined as described in Materials and methods section. Mean ± s.d. values are shown in (c) (*n* = 5). Open boxes, WT mice; closed boxes, Pim-3 Tg mice. *P <0.05; **P <0.01 vs WT mice.(d, e and f) Total RNA was extracted from the liver of WT or Pim-3 Tg mice at the indicated time intervals after DEN treatment and were subjected to a semi-quantitative RT–PCR analysis for the detection of mRNA for interleukin (IL)-1α (d), IL-1β (e), and tumor necrosis factor (TNF)-α (f). The ratio of each cytokine was calculated as described in Materials and methods section. Each value represents mean ± s.d. value (*n* = 5). Open boxes, WT mice; closed boxes, Pim-3 Tg mice. *P <0.05; **P <0.01 vs WT mice.

approximately half of male WT mice developed HCC nodules at 10 months after DEN injection (Figures 5b–d), consistent with the previous report (Yang *et al.*, 2006). In contrast, most Pim-3 transgenic mice developed HCC nodules by 10 months after DEN treatment, with higher relative liver weight and larger numbers of HCC nodules than WT mice (Figures 5b–e). The enhanced hepatocarcinogenesis in Pim-3 transgenic mice may mirror the fact that neovascularization, an essential process for hepatocarcinogenesis, was augmented in Pim-3 transgenic mice compared with that observed for WT mice, as demonstrated by increases in CD31-positive areas in the liver (Figures 5f and g).

Discussion

We previously observed that Pim-3 was expressed selectively in pre-malignant and malignant lesions of the mouse HCC model in transgenic mice expressing hepatitis B virus surface antigen (Fujii *et al.*, 2005). Moreover, Pim-3 protein was detected in a substantial proportion of HCC cells and precancerous lesions in human liver samples, but not normal human liver. Furthermore, Pim-3 protein was also detected in regenerating bile ductules that are assumed to be the proliferation of hepatic stem cells after chronic injury. These observations suggested potential roles of aberrantly expressed Pim-3 in hepatocarcinogenesis. To
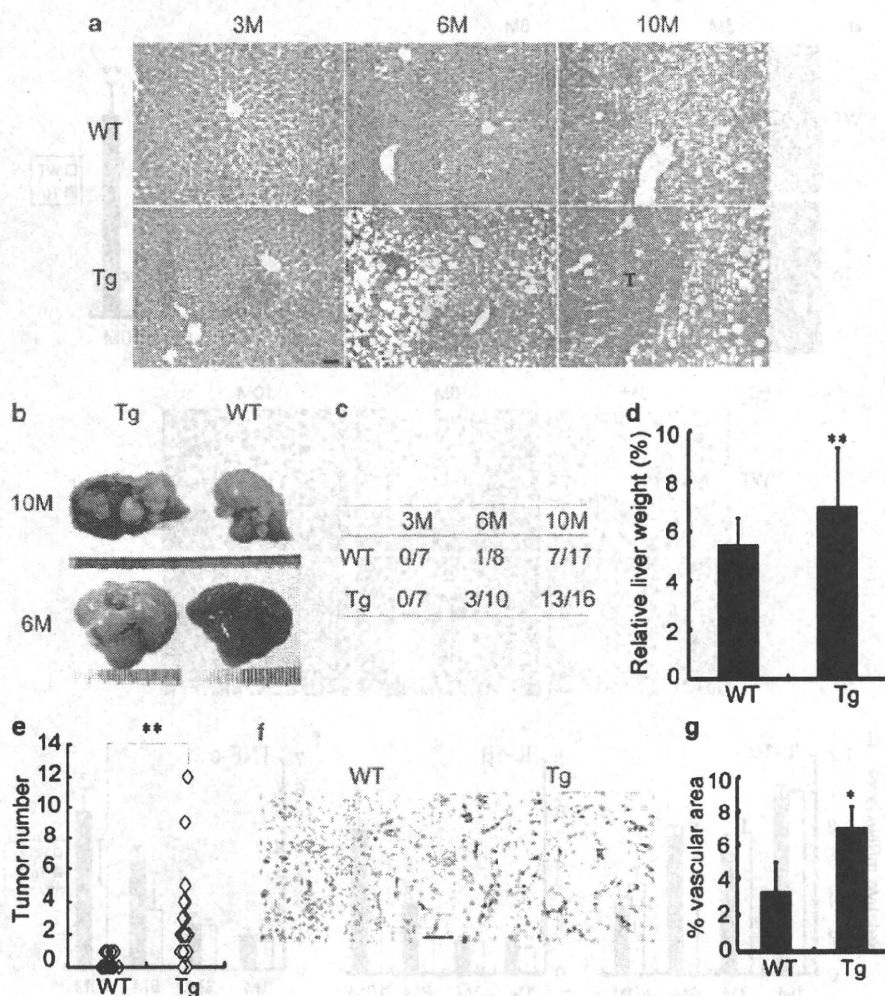
Figure 5 Enhanced hepatocarcinogenesis in Pim-3 transgenic (Tg) mice. (**a**) The liver tissues were obtained from wild-type (WT) or Pim-3 Tg mice at the indicated time intervals after DEN treatment and subjected to hematoxylin and eosin (HE) staining. Representative results from five individual animals are shown here with an original magnification $\times 200$. (**b**) Macroscopic appearance of liver at 10 and 6 months after DEN treatment. Representative results from eight animals are shown here. Left panels: Pim-3 Tg mice; right panels: WT mice. The arrow indicates a small tumor nodule. (**c**) Incidence of macroscopic tumor formation at the indicated time intervals after DEN treatment in WT and Pim-3 Tg mice. (**d**) Liver weight relative to whole body weight was determined for WT and Pim-3 Tg mice at 10 months after DEN treatment. Each value represents mean $\pm$ s.d. value ($n=5$). **$P<0.01$ vs WT mice. (**e**) Numbers of tumors with a diameter of larger than 1 mm were determined in the livers of WT ($n=17$) or Pim-3 Tg mice ($n=16$) at 10 months after DEN treatment. Each symbol indicates the tumor numbers of each animal and the bars represent the median of each group. **$P<0.01$ vs WT mice. (**f** and **g**) The liver tissues were obtained from WT or Pim-3 Tg mice at 10 months after DEN treatment and were subjected to immunostaining with anti-CD31 antibody. Representative results from five individual animals are shown in (**f**) with an original magnification $\times 400$. CD31-positive vascular areas within tumors were determined as described in Materials and methods section. Mean and s.d. values were calculated and are shown in (**g**). *$P<0.05$ vs WT mice.

address the roles of Pim-3, we generated transgenic mice that constitutively express human Pim-3 selectively in liver. Untreated hepatocytes derived from these transgenic mice exhibited enhanced cell proliferation compared with those obtained from WT mice. However, these transgenic mice did not develop HCC spontaneously. Hence, enhanced cell proliferation cannot *per se* result in carcinogenesis in liver.

Kinase activation generally requires a posttranslational modification, particularly, phosphorylation in its regulatory domain. However, another member of the

Pim kinase family, Pim-1, is constitutively active without any further alteration in its conformation because it lacks any regulatory domain (Qian *et al.*, 2005). Similarly, Pim-3 lacks any regulatory domain (Fujii *et al.*, 2005) and *Pim-3* complementary DNA (cDNA) alone induced phosphorylation of its target protein, Bad, at Ser[112] when it was transfected into human pancreatic cancer cell lines (Li *et al.*, 2006). Consistently, Pim-3 transgenic mice exhibited enhanced phosphorylation of Bad at Ser[112] in the liver. The proapoptotic activity of Bad is regulated by its phosphorylation at

Ser^{112} or Ser^{136} (She et al., 2005). Unphosphorylated Bad binds and eventually inactivates anti-apoptotic family members, primarily $Bcl-X_L$ and even Bcl-2 (Yang et al., 1995; Zha et al., 1996). As phosphorylation of Bad at Ser^{112} or Ser^{136} can result in the liberation of $Bcl-X_L$ and Bcl-2, which can prevent apoptosis (Chen et al., 2005), phosphorylated Bad represents its inactive form. However, both WT and Pim-3 transgenic mice developed apoptosis in liver to a similar extent when they were treated with a potent hepatocarcinogen, DEN. These observations suggest that phosphorylated Bad is not sufficient to prevent apoptosis induced by potent hepato-cytotoxic drugs such as DEN.

Pim-3 transgenic mice developed HCC with a higher incidence and a heavier burden than WT mice when both were treated similarly with DEN. Hepatocytes, particularly those in the centrilobular region, metabolized DEN into an alkylating agent that, in turn, can induce DNA damage and mutations in hepatocytes (Verna et al., 1996). Simultaneously, DEN metabolites can generate reactive oxygen species (ROS) (Kamata et al., 2005; Schwabe and Brenner, 2006). When treated with DEN, mice with liver-specific deletion of an essential kinase for NF-κB activation, IKKβ, generated increased levels of ROS in hepatocytes, together with enhanced hepatocyte death and augmented compensatory hepatocyte proliferation. The net result was exaggerated HCC development with a high cell proliferation rate as evidenced by increased PCNA- and cyclin D1-positive cell numbers in liver (Maeda et al., 2005). Similarly, DEN treatment augmented hepatocyte proliferation but not apoptosis in Pim-3 transgenic mice compared with that observed in WT mice, as evidenced by increased PCNA- and cyclin D1-positive cell numbers in liver. These data may account for accelerated hepatocarcinogenesis in Pim-3 transgenic mice. However, several lines of evidence indicate the potential involvement of other Pim kinases, Pim-1 and Pim-2, in NF-κB activation (Hammerman et al., 2004; Zemskova et al., 2008). Thus, it still remains to be investigated whether the Pim-3 transgene can induce ROS generation in a similar manner as the IKKβ deletion.

Liver injury causes liver regeneration primarily through hepatocyte division but if hepatocyte division is impaired, liver repair requires the recruitment of hepatic oval cells (Ma et al., 2006). Oval cells mainly express α-fetoprotein but not albumin, and can proliferate and differentiate into both hepatocytes and bile duct cells. Several independent groups claimed that HCC cells can arise from oval cells (Braun et al., 1989). Mice deficient in the IKKβ gene in liver developed HCC with an incidence higher than WT mice (Maeda et al., 2005). In this mouse, the IKKβ gene was deleted by using cre recombinase expressed under the control of an albumin promoter/enhancer and therefore, the gene was deleted selectively in albumin-expressing hepatocytes but not in oval cells. As we used the same promoter/enhancer to prepare transgenic mice, it is likely that the Pim-3 transgene was expressed selectively in hepatocytes but not in oval cells. Thus, the Pim-3 transgene mainly acted on hepatocytes to promote carcinogenesis,

although its effects on oval cell proliferation cannot completely be excluded.

Accumulating evidence indicates that Pim-1, a member of the Pim kinase family, can progress cell cycle by phosphorylating several cell cycle regulators and altering their activities. Pim-1 can phosphorylate the phosphatase, Cdc25A, thereby increasing its phosphatase activity (Mochizuki et al., 1999). Moreover, Pim-1 can phosphorylate G1-specific inhibitor p21 (Waf), a cyclin-dependent kinase inhibitor, and induce its cytoplasmic localization (Wang et al., 2002). Furthermore, Pim-1 can phosphorylate the kinase Cdc25C-associated kinase (C-TAK)-1 and decrease its kinase activity (Bachmann et al., 2004), whereas Pim-1 can phosphorylate and activate the G2/M-specific phosphatase Cdc25C. Alteration of the activities of these molecules can result in cell cycle progression, particularly during the G2/M phase. Pim-3 and Pim-1, but not Pim-2, bind to a consensus peptide substrate (AKRRRHPSGPPTA) with a strikingly high affinity, having K_d value in the range of 40–60 nM (Bullock et al., 2005). Thus, it is likely that Pim-3 can phosphorylate these cell cycle regulators similarly as Pim-1. Supporting this idea, recombinant Pim-3 protein can phosphorylate p21/Waf in vitro (Morishita et al., 2008). This may account for the observations that cell cycle progression was accelerated in Pim-3 transgenic mouse-derived hepatocytes compared with WT mice, as evidenced by increased proportion of the cells in G2/M phase and reciprocally decreased proportion of the cells in G0/G1 phase.

The hepatocarcinogen, DEN, induced TNF-α production consistently with the previous report (Sakurai et al., 2006) and the production was further augmented by Pim-3 overexpression in liver. The crucial involvement of TNF-α in hepatocyte proliferation was proposed by the observation that liver regeneration after partial hepatectomy was impaired in mice deficient in TNF receptor gene (Yamada et al., 1997). Moreover, accumulating evidence indicates the potential contribution of TNF-α to hepatocarcinogenesis (Roberts and Kimber, 1999; Schwabe and Brenner, 2006). Furthermore, TNF-α can promote angiogenesis, an essential process for tumorigenesis, by inducing the production of angiogenic factors, such as vascular endothelial growth factor and hepatocyte growth factor (Tamura et al., 1993; Yoshida et al., 1997). The production of TNF-α was regulated at several steps and the first one was at the transcription level, governed by transcription factors, such as NF-κB and Activator protein-1AP-1 (Manna et al., 2000; Udalova and Kwiatkowski, 2001; Chung et al., 2007). As Pim-1 can enhance NF-κB transcriptional activity (Zemskova et al., 2008), Pim-3 might be able to similarly activate NF-κB, thereby inducing TNF-α expression.

It is most likely that our transgenic mice expressed a high level of the Pim-3 transgene selectively in hepatocytes. A strong similarity of Pim-3 with another Pim kinase, Pim-1, suggests that Pim-3 can phosphorylate several cell cycle regulators and accelerate cell cycle progression as Pim-1 does. In support of this idea, we observed enhanced cell cycle progression in untreated

Pim-3 transgenic mouse-derived hepatocytes compared with that observed for WT mice. However, as evidenced by the absence of spontaneous HCC development in Pim-3 transgenic mice, accelerated hepatocyte proliferation alone cannot induce HCC. The hepatocarcinogen, DEN, can generate O^6-methlguanine and can frequently induce G-C-to-A-T transition mutations in hepatocytes (Nakatsuru et al., 1993). The Pim-3 transgene can enhance the proliferation of hepatocytes through G-C-to-A-T transition mutations, thereby accelerating HCC development. We previously observed that Pim-3 expression was detected in pre-malignant and malignant lesions but not in normal tissues of liver in humans and mice (Fujii et al., 2005). Thus, Pim-3 may be a promoter but not an initiator of HCC development, and blocking of Pim-3 activity can delay and/or prevent HCC development.

Materials and methods

Preparation of Pim-3 transgenic mice
The mouse albumin enhancer/promoter region (Figure 1a) was a kind gift from Dr Palmiter (University of Washington, Seattle, WA, USA; Pinkert et al., 1987). Full-length human Pim-3 cDNA was subcloned 3 to this albumin enhancer/promoter gene. After being linearized by digestion with NotI, the gene was introduced into fertilized oocytes of C57BL/6 mice using a standard transgenic technique. Genomic DNA was isolated from the tail of the founder and offspring using Nucleospin tissue kit (Macherey Nagel, Düren, Germany) and genotyping was performed by PCR using a specific pair of primers, including a sense primer (5'-TTGAACTCATCGACC TGCAGGCAT-3') flanking the upstream albumin promoter and an antisense primer (5'-GCCTTCTCGAAGCTCTCCTT GTCC-3') inside the human Pim-3 cDNA. Transgenic founder animals were mated with C57BL/6 mice (Charles River Japan, Yokohama, Japan). The male offspring with a heterozygous transgene were used as a transgenic group, whereas those without a transgene were used as a littermate control. All mice were kept under the specific pathogen-free conditions, and all animal experiments in this study complied with the Guidelines of the Care and Use of Laboratory Animals of Kanazawa University.

Hepatocyte isolation
Mouse hepatocytes were isolated by using a two-step perfusion method with some modifications. Briefly, under anesthetization with Avertin (2,2,2-tribromoethanol; Sigma-Aldrich, St Louis, MO, USA), a needle was inserted along the inferior vena cava and the liver was perfused sequentially with phosphate-buffered saline and collagenase-containing buffer at a rate of 5–10 ml/min. The liver was then dissected, suspended in ice-cold phosphate-buffered saline and filtered through a cell strainer with a pore size of 100 μm to remove connective tissue debris and cell clumps. After the cell suspensions were left on ice for 15 min, the resultant precipitates were collected, suspended in DMEM medium (Sigma-Aldrich) and centrifuged at 800 r.p.m. for 2 min. Cell suspensions were further centrifuged in 45% Percoll solution (Sigma-Aldrich) at 1000 r.p.m. for 10 min. The obtained cells were confirmed to consist of more than 95% hepatocytes on the basis of morphological criteria, with a viability of higher than 90% on trypan blue exclusion test. Purified hepatocytes

were used for the following DNA content analysis and immunoblotting analysis.

Cell cycle analysis
The obtained hepatocytes were fixed with 70% ethanol at −20 °C. The fixed cells were incubated with 50 μg/ml propidium iodine (Molecular Probes, Eugene, OR, USA) and 1 μg/ ml RNase A for 30 min at room temperature. The DNA content was then analyzed on a FACS Calibur system (BD Biosciences, Bedford, MA, USA). The distribution of cells in each cell-cycle phase was determined by cell ModFit LT software (BD Biosciences).

Protein extraction and western blotting
Hepatocytes or liver tissues were obtained and homogenized with RIPA buffer (Santa Cruz Biotechnology, Santa Cruz, CA, USA) containing proteinase inhibitor cocktail (Roche Diagnostics AG, Rotkreutz, Switzerland). After sonication for 1 min, homogenates were centrifuged at 15 000 g for 15 min at 4 °C to obtain the supernatants. After total protein concentrations were measured using a BCA kit (Pierce Biotechnology, Rockford, IL, USA), resultant supernatants were subjected to immunoblotting using anti-phospho-Ser[112]-Bad, anti-phospho-Ser[136]-Bad, anti-Bad, anti-Pim-3, anti-β actin (Sigma-Aldrich); anti-cyclin D1 (Cell Signaling Technology, Beverly, MA, USA) and anti-PCNA antibodies (BD Biosciences) as previously described (Li et al., 2006).

Chemical-induced liver injury and subsequent hepatocarcinogenesis
Three-week old weaning mice were given a single intraperitoneal injection of DEN (Sigma-Aldrich), dissolved in physiological saline solution at a dose 10 mg/kg body weight as previously described (Yang et al., 2006), to induce hepatocarcinogenesis. To induce acute liver injury, mice were given a dose of 100 mg/kg body weight. Serum alanine amino transferase levels were determined using a Fuji DRICHEM 55500V (Fuji Medical System, Tokyo, Japan) according to the manufacturer's instructions. Mice were killed at the indicated time intervals after the injection to conduct histopathological analysis.

RNA isolation and RT–PCR
Total RNAs were extracted from the organs using RNeasy mini kit (Qiagen, Hilden, Germany) according to the manufacturer's instructions and were further treated with RNase-free DNase (Promega, Madison, WI, USA) to deplete residual contaminated DNA. A total of 2 μg RNA was reverse-transcribed at 42 °C for 1 h in 20-μl reaction mixture containing Moloney murine leukemia virus reverse trancriptase (Toyobo, Osaka, Japan) and hexanucleotide random primer (Qiagen) to obtain cDNA as previously described (Wu et al., 2008). Serially twofold diluted cDNA products were amplified for glyceraldehyde-3-phosphate dehydrogenase (GAPDH) using a specific set of primers (Table 1) using 25 cycles consisting of following reaction conditions: 94 °C for 30 s, 58 °C for 30 s and 72 °C for 1 min in a 25-μl of reaction mixture containing Taq polymerase (Takara Bio, Kyoto, Japan) to evaluate the quantity of the transcribed cDNA. Equal quantities of cDNA products were then amplified for the indicated genes using the specific sets of primers (Table 1) with 35 cycles consisting of following conditions: 94 °C for 30 s, 58 °C for 1 min and 72 °C for 1 min. The resultant PCR products were fractionated on 1.5% agarose gel and visualized by ethidium bromide staining under ultraviolet light trans-

−574−

Table 1 Sequences of the primers used for RT–PCR

Gene Name	Forward	Reverse	Cycles	Length (bp)
Mouse Pim-3	5'-GAGAGGGTCTCCCCAGAGT-3'	5'-TGGTGGCACGCTTAGGTTG-3'	35	660
Human Pim-3	5'-CGGAGGAGGGTCTCTCCAGAGTG-3'	5'-ACCCTGCGCCGGCGGAAAG-3'	35	535
Mouse TNF-α	5'-AGTTCTATGGCCCAGACCCT-3'	5'-CGGACTCCGCAAAGTCTAAG-3'	35	463
Mouse IL-1α	5'-CTCTAGAGCTCCATGCTACAGAC-3'	5'-TGGAATCCAGGGGAA ACACTG-3'	35	309
Mouse IL-1β	5'-ATGGCAACTGTTCCTGAACTCAAC T-3'	5'-CAGGACAGGTATAGATTCTTTCCTTTT-3'	35	377
GADPH	5'-ACCACAGTCCATGCCATCAC-3'	5'-TCCACCACCCTGTTGCTGTA-3'	25	431

Abbreviations: GADPH, glyceraldehydes-3-phosphate dehydrogenase; IL, interleukin; TNF, tumor necrosis factor.

illumination. The band intensities were measured using National Institutes of Health Image analysis software, version 1.62, and the ratios to GAPDH were calculated on the assumption that the ratios of untreated animals were set at 1.0.

Histopathological analysis
The liver tissue was fixed in 10% formalin buffered with phosphate-buffered saline (pH 7.2). and embedded in paraffin. Five-μm thick sections were stained with hematoxylin and eosin solution or subjected to the terminal transferase dUTP nick end labeling assay (MBL, Nagoya, Japan) according to the manufacturer's instructions. Immunohistochemical analysis was performed using anti-PNCA (BD Biosciences) or anti-cleaved caspase-3 antibodies (Cell Signaling Technology). A portion of the liver tissue was snap-frozen, dried at room temperature until the tissues firmly adhered to the slides, and was fixed in cold acetone for 10 min. The sections were blocked with serum-free Protein Block (Dako Cytomation, Glostrup, Denmark) and were incubated with rabbit anti-cyclin B1 antibodies (Santa Cruz Biotechnology). They were further incubated with Alexa Fluor 488-labeled donkey anti-rabbit IgG followed by counterstaining with 4-6-diamidino-2-pheny-lindole (Vector Laboratories, Burlingame, CA, USA) in dark. Immunoflurescence was visualized on a Laser Microscope 510 (Carl Zeiss, Hamburg, Germany) and cyclin B1-positive cell proportion was determined on 10 randomly chosen fields at × 200 magnification. Another slides were used for staining with oil red (Sigma-Aldrich) and hematoxylin counterstaining, or immunohistochemical analysis using anti-CD31 antibodies (BD Pharmingen). The immune complexes were visualized by Envision+ System (Dako Cytomation), a catalyzed signal amplification system or the Elite ABC kit and DAB substrate kit (Vector Laboratories) according to the manufacturer's instructions. The positive cell numbers were enumerated on 10 randomly chosen visual fields at × 400 magnification. The CD31-postive areas were determined as previously described (Wu *et al.*, 2008). In brief, CD31-positive areas in the tumor tissue were defined as the intratumoral vascular areas. Areas of active neovascularization (hot spot) were found inside tumor foci by scanning the section at lower magnification and the pixel numbers of CD31-positive areas were then determined on five randomly chosen fields in hot spots of each animal at × 400 magnification with the help of Photoshop version 7.0. The density of neovascularization was expressed as a percentage of the whole tumor area. All histopathological examinations were conducted by an examiner without any prior knowledge of the experimental procedures. All histopathological examinations were conducted blind, by an examiner without any prior knowledge of the experimental procedures.

Statistical analysis
All obtained data were calculated and expressed as mean ± s.d. The differences were analyzed statistically using one-way analysis of variance, followed by the Turkey–Kramer test. $P < 0.05$ was considered statistically significant.

Conflict of interest

The authors declare no conflict of interest.

References

Bachmann M, Hennemann H, Xing PX, Hoffmann I, Moroy T. (2004). The oncogenic serine/threonine kinase Pim-1 phosphorylates and inhibits the activity of Cdc25C-associated kinase (C-TAK-1): a novel role for Pim-1 at the G2/M cell cycle checkpoint. *J Biol Chem* 279: 48319–48328.

Braun L, Mikumo R, Fausto N. (1989). Production of hepatocellular carcinoma by oval cells: cell cycle expression of c-myc and p53 at different stages of oval cell transformation. *Cancer Res* 49: 1554–1561.

Bullock AN, Debreczeni J, Amos AL, Knapp S, Turk BE. (2005). Structure and substrate specificity of the Pim-1 kinase. *J Biol Chem* 280: 41675–41682.

Chen L, Willis SN, Wei A, Smith BJ, Fletcher JI, Hinds MG *et al.* (2005). Differential targeting of prosurvival Bcl-2 proteins by their BH3-only ligands allows complementary apoptotic function. *Mol Cell* 17: 393–403.

Chung J, Koyama T, Ohsawa M, Shibamiya A, Hoshi A, Hirosawa S. (2007). 1,25(OH)(2)D(3) blocks TNF-induced monocytic tissue factor expression by inhibition of transcription factors AP-1 and NF-kappaB. *Lab Invest* 87: 540–547.

Deneen B, Welford SM, Ho T, Hernandez F, Kurland I, Denny CT. (2003). PIM3 proto-oncogene kinase is a common transcriptional target of divergent EWS/ETS oncoproteins. *Mol Cell Biol* 23: 3897–3908.

Farazi PA, DePinho RA. (2006). Hepatocellular carcinoma pathogenesis: from genes to environment. *Nat Rev Cancer* 6: 674–687.

Feldman JD, Vician L, Crispino M, Tocco G, Marcheselli VL, Bazan NG *et al.* (1998). KID-1, a protein kinase induced by depolarization in brain. *J Biol Chem* 273: 16535–16543.

Fujii C, Nakamoto Y, Lu P, Tsuneyama K, Popivanova BK, Kaneko S *et al.* (2005). Aberrant expression of serine/threonine kinase Pim-3 in hepatocellular carcinoma development and its role in the proliferation of human hepatoma cell lines. *Int J Cancer* 114: 209–218.

Hammerman PS, Fox CJ, Cinalli RM, Xu A, Wagner JD, Lindsten T *et al.* (2004). Lymphocyte transformation by Pim-2 is dependent on nuclear κB activation. *Cancer Res* 64: 8341–8348.

Hosono S, Chou MJ, Lee CS, Shih C. (1993). Infrequent mutation of *p53* gene in hepatitis B virus positive primary hepatocellular carcinomas. *Oncogene* **8**: 491–496.

Kamata H, Honda S, Maeda S, Chang L, Hirata H, Karin M. (2005). Reactive oxygen species promote TNFalpha-induced death and sustained JNK activation by inhibiting MAP kinase phosphatases. *Cell* **120**: 649–661.

Li YY, Popivanova BK, Nagai Y, Ishikura H, Fujii C, Mukaida N. (2006). Pim-3, a proto-oncogene with serine/threonine kinase activity, is aberrantly expressed in human pancreatic cancer and phosphorylates bad to block bad-mediated apoptosis in human pancreatic cancer cell lines. *Cancer Res* **66**: 6741–6747.

Ma W, Xia X, Stafford LJ, Yu C, Wang F, LeSage G et al. (2006). Expression of GCIP in transgenic mice decreases susceptibility to chemical hepatocarcinogenesis. *Oncogene* **25**: 4207–4216.

Maeda S, Kamata H, Luo JL, Leffert H, Karin M. (2005). IKKbeta couples hepatocyte death to cytokine-driven compensatory proliferation that promotes chemical hepatocarcinogenesis. *Cell* **121**: 977–990.

Manna SK, Mukhopadhyay A, Aggarwal BB. (2000). Leflunomide suppresses TNF-induced cellular responses: effects on NF-kappa B, activator protein-1, c-Jun N-terminal protein kinase, and apoptosis. *J Immunol* **165**: 5962–5969.

Mochizuki T, Kitanaka C, Noguchi K, Muramatsu T, Asai A, Kuchino Y. (1999). Physical and functional interactions between Pim-1 kinase and Cdc25A phosphatase. Implications for the Pim-1-mediated activation of the c-Myc signaling pathway. *J Biol Chem* **274**: 18659–18666.

Morishita D, Katayama R, Sekimizu K, Tsuruo T, Fujita N. (2008). Pim kinases promote cell cycle progression by phosphorylating and down-regulating p27Kip1 at the transcriptional and posttranscriptional levels. *Cancer Res* **68**: 5076–5085.

Nakatsuru Y, Matsukuma S, Nemoto N, Sugano H, Sekiguchi M, Ishikawa T. (1993). O⁶-methylguanine-DNA methyltransferase protects against nitrosamine-induced hepatocarcinogenesis. *Proc Natl Acad Sci USA* **90**: 6468–6472.

Otani K, Korenaga M, Beard MR, Li K, Qian T, Showalter LA et al. (2005). Hepatitis C virus core protein, cytochrome P450 2E1, and alcohol produce combined mitochondrial injury and cytotoxicity in hepatoma cells. *Gastroenterology* **128**: 96–107.

Pinkert CA, Ornitz DM, Brinster RL, Palmiter RD. (1987). An albumin enhancer located 10 kb upstream functions along with its promoter to direct efficient, liver-specific expression in transgenic mice. *Genes Dev* **1**: 268–276.

Popivanova BK, Li YY, Zheng H, Omura K, Fujii C, Tsuneyama K et al. (2007). Proto-oncogene, Pim-3 with serine/threonine kinase activity, is aberrantly expressed in human colon cancer cells and can prevent Bad-mediated apoptosis. *Cancer Sci* **98**: 321–328.

Qian KC, Wang L, Hickey ER, Studts J, Barringer K, Peng C et al. (2005). Structural basis of constitutive activity and a unique nucleotide binding mode of human Pim-1 kinase. *J Biol Chem* **280**: 6130–6137.

Roberts RA, Kimber I. (1999). Cytokines in genotoxic hepatocarcinogenesis. *Carcinogenesis* **20**: 1297–1401.

Sakurai T, Maeda S, Chang L, Karin M. (2006). Loss of hepatic NF-kappa B activity enhances chemical hepatocarcinogenesis through sustained c-Jun N-terminal kinase 1 activation. *Proc Natl Acad Sci USA* **103**: 10544–10551.

Schwabe RF, Brenner DA. (2006). Mechanisms of liver injury. I. TNF-alpha-induced liver injury: role of IKK, JNK, and ROS pathways. *Am J Physiol Gastrointest Liver Physiol* **290**: G583–G589.

She QB, Solit DB, Ye Q, O'Reilly KE, Lobo J, Rosen N. (2005). The BAD protein integrates survival signaling by EGFR/MAPK and PI3K/Akt kinase pathways in PTEN-deficient tumor cells. *Cancer Cell* **8**: 287–297.

Tamura M, Arakaki N, Tsuboushi H, Takada H, Daikuhara Y. (1993). Enhancement of human hepatocyte growth factor production by interleukin-1α and -1β and tumor necrosis factor-α by fibroblasts in culture. *J Biol Chem* **268**: 8140–8145.

Thorgeirsson SS, Grisham JW. (2002). Molecular pathogenesis of human hepatocellular carcinoma. *Nat Genet* **31**: 339–346.

Udalova IA, Kwiatkowski D. (2001). Interaction of AP-1 with a cluster of NF-kappa B binding elements in the human TNF promoter region. *Biochem Biophys Res Commun* **289**: 25–33.

Umemura T, Ichijo T, Yoshizawa K, Tanaka E, Kiyosawa K. (2009). Epidemiology of hepatocellular carcinoma in Japan. *J Gastroenterol* **44**(Suppl 19): 102–107.

Verna L, Whysner J, Williams GM. (1996). N-nitrosodiethylamine mechanistic data and risk assessment: bioactivation, DNA-adduct formation, mutagenicity, and tumor initiation. *Pharmacol Ther* **71**: 57–81.

Wang Y, Ausman LM, Greenberg AS, Russel RM, Wang X-D. (2009). Nonalcoholic steatohepatitis induced by a high-fat diet promotes diethylnitrosamine-initiated early hepatocarcinogenesis in rats. *In t J Cancer* **124**: 540–546.

Wang Z, Bhattacharya N, Mixter PF, Wei W, Sedivy J, Magnuson NS. (2002). Phosphorylation of the cell cycle inhibitor p21Cip1/WAF1 by Pim-1 kinase. *Biochim Biophys Acta* **1593**: 45–55.

Wu Y, Li YY, Matsushima K, Baba T, Mukaida N. (2008). CCL3–CCR5 axis regulates intratumoral accumulation of leukocytes and fibroblasts and promotes angiogenesis in murine lung metastasis process. *J Immunol* **181**: 6384–6393.

Yamada Y, Kirillova I, Peschon JJ, Fausto N. (1997). Initiation of liver growth by tumor necrosis factor: deficient liver regeneration in mice lacking type I tumor necrosis factor receptor. *Proc Natl Acad Sci USA* **94**: 1441–1446.

Yang E, Zha J, Jockel J, Boise LH, Thompson CB, Korsmeyer SJ. (1995). Bad, a heterodimeric partner for Bcl-XL and Bcl-2, displaces Bax and promotes cell death. *Cell* **80**: 285–291.

Yang X, Lu P, Fujii C, Nakamoto Y, Gao JL, Kaneko S et al. (2006). Essential contribution of a chemokine, CCL3, and its receptor, CCR1, to hepatocellular carcinoma progression. *Int J Cancer* **118**: 1869–1876.

Yoshida S, Ono M, Shono T, Izumi H, Ishibashi T, Suzuki H et al. (1997). Involvement of interleukin-8, vascular endothelial growth factor, and basic fibroblast growth factor in tumor necrosis factor α-dependent angiogenesis. *Mol Cell Biol* **17**: 4015–4023.

Zemskova M, Sahakian E, Bashkirova S, Lilly M. (2008). The PIM1 kinase is a critical component of a survival pathway activated by docetaxel and promotes survival of docetaxel-treated prostate cancer cells. *J Biol Chem* **283**: 20635–20644.

Zha J, Harada H, Yang E, Jockel J, Korsmeyer SJ. (1996). Serine phosphorylation of death agonist BAD in response to survival factor results in binding to 14-3-3 not BCL-X(L). *Cell* **87**: 619–628.

Zheng HC, Tsuneyama K, Takahashi H, Miwa S, Sugiyama T, Popivanova BK et al. (2008). Aberrant Pim-3 expression is involved in gastric adenoma-adenocarcinoma sequence and cancer progression. *J Cancer Res Clin Oncol* **134**: 481–488.

Zheng Y, Chen WL, Louie SG, Yen TS, Ou JH. (2007). Hepatitis B virus promotes hepatocarcinogenesis in transgenic mice. *Hepatology* **45**: 16–21.

Prolonged recurrence-free survival following OK432-stimulated dendritic cell transfer into hepatocellular carcinoma during transarterial embolization

Y. Nakamoto,* E. Mizukoshi,*
M. Kitahara,* F. Arihara,* Y. Sakai,*
K. Kakinoki,* Y. Fujita,*
Y. Marukawa,* K. Arai,*
T. Yamashita,* N. Mukaida,†
K. Matsushima,‡ O. Matsui§ and
S. Kaneko*

*Disease Control and Homeostasis, Graduate School of Medicine, †Division of Molecular Bioregulation, Cancer Research Institute, Kanazawa University, §Department of Radiology, Graduate School of Medicine, Kanazawa University, Kanazawa, and ‡Department of Molecular Preventive Medicine, Graduate School of Medicine, University of Tokyo, Tokyo, Japan

Summary

Despite curative locoregional treatments for hepatocellular carcinoma (HCC), tumour recurrence rates remain high. The current study was designed to assess the safety and bioactivity of infusion of dendritic cells (DCs) stimulated with OK432, a streptococcus-derived anti-cancer immunotherapeutic agent, into tumour tissues following transcatheter hepatic arterial embolization (TAE) treatment in patients with HCC. DCs were derived from peripheral blood monocytes of patients with hepatitis C virus-related cirrhosis and HCC in the presence of interleukin (IL)-4 and granulocyte-macrophage colony-stimulating factor and stimulated with 0·1 KE/ml OK432 for 2 days. Thirteen patients were administered with 5×10^6 of DCs through arterial catheter during the procedures of TAE treatment on day 7. The immunomodulatory effects and clinical responses were evaluated in comparison with a group of 22 historical controls treated with TAE but without DC transfer. OK432 stimulation of immature DCs promoted their maturation towards cells with activated phenotypes, high expression of a homing receptor, fairly well-preserved phagocytic capacity, greatly enhanced cytokine production and effective tumoricidal activity. Administration of OK432-stimulated DCs to patients was found to be feasible and safe. Kaplan–Meier analysis revealed prolonged recurrence-free survival of patients treated in this manner compared with the historical controls ($P = 0·046$, log-rank test). The bioactivity of the transferred DCs was reflected in higher serum concentrations of the cytokines IL-9, IL-15 and tumour necrosis factor-α and the chemokines CCL4 and CCL11. Collectively, this study suggests that a DC-based, active immunotherapeutic strategy in combination with locoregional treatments exerts beneficial anti-tumour effects against liver cancer.

Keywords: dendritic cells, hepatocellular carcinoma, immunotherapy, recurrence-free survival, transcatheter hepatic arterial embolization

Introduction

Many locoregional therapeutic approaches including surgical resection, radiofrequency ablation (RFA) and transcatheter hepatic arterial embolization (TAE) have been taken in the search for curative treatments of hepatocellular carcinoma (HCC). Despite these efforts, tumour recurrence rates remain high [1,2], probably because active hepatitis and cirrhosis in the surrounding non-tumour liver tissues causes *de novo* development of HCC [3,4]. One strategy to reduce tumour recurrence is to enhance anti-tumour immune responses that may induce sufficient inhibitory effects to prevent tumour cell growth and survival [5,6]. Dendritic

cells (DCs) are the most potent type of antigen-presenting cells in the human body, and are involved in the regulation of both innate and adaptive immune responses [7]. DC-based immunotherapies are believed to contribute to the eradication of residual and recurrent tumour cells.

To enhance tumour antigen presentation to T lymphocytes, DCs have been transferred with major histocompatibility complex (MHC) class I and class II genes [8] and co-stimulatory molecules, e.g. CD40, CD80 and CD86 [9,10], and loaded with tumour-associated antigens, including tumour lysates, peptides and RNA transfection [11]. To induce natural killer (NK) and natural killer T (NK T) cell activation, DCs have been stimulated and modified to

Table 1. Patient characteristics.

Patient no.	Gender	Age (years)	HLA	TNM stages	No. of tumours	Largest tumour (mm)	Child–Pugh	KPS	Post-TAE Rx
1	M	60	A11 A33	III	5	35	B	100	RFA
2	M	57	A11 A24	III	1	21	B	100	RFA
3	M	57	A11 A31	III	2	39	B	100	RFA
4	M	77	A2 A24	III	2	35	A	100	RFA
5	F	83	A11 A24	III	3	29	B	100	RFA
6	F	74	A2 A24	II	1	35	A	100	RFA
7	F	72	A24 A33	III	3	41	B	100	RFA
8	F	65	A2 A11	II	4	12	B	100	RFA
9	M	71	A2 A11	II	4	16	A	100	RFA
10	M	79	A11 A24	III	2	40	A	100	RFA
11	M	71	A2 A24	II	1	28	A	100	RFA
12	M	56	A2 A26	III	2	25	B	100	RFA
13	M	64	A2 A33	III	2	37	B	100	RFA

M, male; F, female; TNM, tumour–node–metastasis; Child–Pugh, Child–Pugh classification; KPS, Karnofsky performance scores; TAE, transcatheter arterial embolization; Rx, treatment; HCC, hepatocellular carcinoma; HLA, human leucocyte antigen; RFA, percutaneous radiofrequency ablation.

produce larger amounts of cytokines, e.g. interleukin (IL)-12, IL-18 and type I interferons (IFNs)[10,12]. Furthermore, DC migration into secondary lymphoid organs could be induced by expression of chemokine genes, e.g. C-C chemokine receptor-7 (CCR7) [13], and by maturation using inflammatory cytokines [14], matrix metalloproteinases and Toll-like receptor (TLR) ligands [15].

DCs stimulated with OK432, a penicillin-inactivated and lyophilized preparation of Streptococcus pyogenes, were suggested recently to produce large amounts of T helper type 1 (Th1) cytokines, including IL-12 and IFN-γ and enhance cytotoxic T lymphocyte activity compared to a standard mixture of cytokines [tumour necrosis factor-α (TNF-α), IL-1β, IL-6 and prostaglandin E$_2$ (PGE$_2$)] [16]. Furthermore, because OK432 modulates DC maturation through TLR-4 and the β_2 integrin system [16,17] and TLR-4-stimulated DCs can abrogate the activity of regulatory T cells [18], OK432-stimulated DCs may contribute to the induction of anti-tumour immune responses partly by reducing the activity of suppressor cells. Recently, in addition to the orchestration of immune responses, OK432-activated DCs have themselves been shown to mediate strong, specific cytotoxicity towards tumour cells via CD40/CD40 ligand interactions [19].

We have reported recently that combination therapy using TAE together with immature DC infusion is safe for patients with cirrhosis and HCC [20]. DCs were infused precisely into tumour tissues and contributed to the recruitment and activation of immune cells in situ. However, this approach by itself yielded limited anti-tumour effects due probably to insufficient stimulation of immature DCs (the preparation of which seems closely related to therapeutic outcome [21,22]). The current study was designed to assess the safety and bioactivity of OK432-stimulated DC infusion into tumour tissues following TAE treatment in patients with cirrhosis and HCC. In addition to documenting the safety of

this approach, we found that patients treated with OK432-stimulated DCs displayed unique cytokine and chemokine profiles and, most importantly, experienced prolonged recurrence-free survival.

Patients and methods

Patients

Inclusion criteria were a radiological diagnosis of primary HCC by computed tomography (CT) angiography, hepatitis C virus (HCV)-related HCC, a Karnofsky score of $\geq$ 70%, an age of $\geq$ 20 years, informed consent and the following normal baseline haematological parameters (within 1 week before DC administration): haemoglobin $\geq$ 8·5 g/dl; white cell count $\geq$ 2000/μl; platelet count $\geq$ 50 000/μl; creatinine < 1·5 mg/dl and liver damage A or B [23].

Exclusion criteria included severe cardiac, renal, pulmonary, haematological or other systemic disease associated with a discontinuation risk; human immunodeficiency virus (HIV) infection; prior history of other malignancies; history of surgery, chemotherapy or radiation therapy within 4 weeks; immunological disorders including splenectomy and radiation to the spleen; corticosteroid or anti-histamine therapy; current lactation; pregnancy; history of organ transplantation; or difficulty in follow-up.

Thirteen patients (four women and nine men) presenting at Kanazawa University Hospital between March 2004 and June 2006 were enrolled into the study, with an age range from 56 to 83 years (Table 1). Patients with verified radiological diagnoses of HCC stage II or more were eligible and enrolled in this study. In addition, a group of 22 historical controls (nine women and 13 men) treated with TAE without DC administration between July 2000 and September 2007 was included in this study. All patients received RFA therapy to increase the locoregional effects 1 week later [24].

They underwent ultrasound, computed tomography (CT) scan or magnetic resonance imaging (MRI) of the abdomen about 1 month after treatment and at a minimum of once every 3 months thereafter, and tumour recurrences were followed for up to 360 days. The Institutional Review Board reviewed and approved the study protocol. This study complied with ethical standards outlined in the Declaration of Helsinki. Adverse events were monitored for 1 month after the DC infusion in terms of fever, vomiting, abdominal pain, encephalopathy, myalgia, ascites, gastrointestinal disorder, bleeding, hepatic abscess and autoimmune diseases.

Preparation and injection of autologous DCs

DCs were generated from blood monocyte precursors, as reported previously [25]. Briefly, peripheral blood mononuclear cells (PBMCs) were isolated by centrifugation in Lymphoprep™ Tubes (Nycomed, Roskilde, Denmark). For generating DCs, PBMCs were plated in six-well tissue culture dishes (Costar, Cambridge, MA, USA) at 1.4×10^7 cells in 2 ml per well and allowed to adhere to plastic for 2 h. Adherent cells were cultured in serum-free media (GMP CellGro® DC Medium; CellGro, Manassas, VA, USA) with 50 ng/ml recombinant human IL-4 (GMP grade; CellGro®) and 100 ng/ml recombinant human granulocyte–macrophage colony-stimulating factor (GM-CSF) (GMP grade; Cell-Gro®) for 5 days to generate immature DC, and matured for a further 2 days in 0.1 KE/ml OK432 (Chugai Pharmaceuticals, Tokyo, Japan) to generate OK-DC. On day 7, the cells were harvested for injection, 5×10^6 cells were suspended in 5 ml normal saline containing 1% autologous plasma, mixed with absorbable gelatin sponge (Gelfoam; Pharmacia & Upjohn, Peapack, NJ, USA) and infused through an arterial catheter following Lipiodol (iodized oil) (Lipiodol Ultrafluide, Laboratoire Guerbet, Aulnay-Sous-Bois, France) injection during selective TAE therapy. Release criteria for DCs were viability > 80%, purity > 30%, negative Gram stain and endotoxin polymerase chain reaction (PCR) and negative in process cultures from samples sent 48 h before release. All products met all release criteria, and the DCs had a typical phenotype of CD14⁻ and human leucocyte antigen (HLA)-DR⁺.

Flow cytometry analysis

The DC preparation was assessed by staining with the following monoclonal antibodies for 30 min on ice: anti-lineage cocktail 1 (lin-1; CD3, CD14, CD16, CD19, CD20 and CD56)-fluorescein isothiocyanate (FITC), anti-HLA-DR-peridinin chlorophyll protein (PerCP) (L243), anti-CCR7-phycoerythrin (PE) (3D12) (BD PharMingen, San Diego, CA, USA), anti-CD80-PE (MAB104), anti-CD83-PE (HB15a) and anti-CD86-PE (HA5.2B7) (Beckman Coulter, Fullerton, CA, USA). Cells were analysed on a fluorescence activated cell sorter (FACS0Calibur™ flow cytometer. Data

analysis was performed with CELLQuest™ software (Becton Dickinson, San Jose, CA, USA).

DC phagocytosis

Immature DCs and OK432-stimulated DCs were incubated with 1 mg/ml FITC dextran (Sigma-Aldrich, St Louis, MO, USA) for 30 min at 37°C and the cells were washed three times in FACS buffer before cell acquisition using a FACS-Calibur™ cytometer. Control DCs (not incubated with FITC dextran) were acquired at the same time to allow background levels of fluorescence to be determined.

Enzyme-linked immunosorbent assay (ELISA)

DCs were seeded at 200 000 cells/ml, and supernatant collected after 48 h. IL-12p40 and IFN-γ were detected using matched paired antibodies (BD Pharmingen) following standard protocols.

Cytotoxicity assays

The ability of DCs to exert cytotoxicity was assessed in a standard ^{51}Cr release assay [19]. We used the HCC cell lines Hep3B and PLC/PRF/5 [American Type Culture Collection (ATCC), Manassas, VA, USA] and a lymphoblastoid cell line T2 that expresses HLA-A*0201 (ATCC) as target cells. Target cells were labelled with ^{51}Cr. In a 96-well plate, 2.5×10^3 target cells per well were incubated with DCs for 8 h at different effector/target (E/T) ratios in triplicate. Percentage of specific lysis was calculated as follows: (experimental release – spontaneous release)/(maximum release – spontaneous release) $\times$ 100. Spontaneous release was always < 20% of the total.

NK cell activity

NK cell cytotoxicity against K562 erythroleukemia target cells was measured by using ^{51}Cr-release assay, according to previously published methods [26], with PBMCs obtained from the patients. All experiments were performed in triplicate. Percentage of cytotoxicity was calculated as follows: {[experimental counts per minute (cpm) – spontaneous cpm]/[total cpm – spontaneous cpm]} $\times$ 100.

Intracellular cytokine expression

Freshly isolated PBMCs were stimulated with 25 ng/ml phorbol 12-myristate 13-acetate (PMA; Sigma-Aldrich) and 1 μg/ml ionomycin (Sigma-Aldrich) at 37°C in humidified 7% CO_2 for 4 h. To block cytokine secretion, brefeldin A (Sigma) [27] was added to a final concentration of 10 μg/ml. After addition of stimuli, the surface staining was performed with anti-CD4-PC5 (13B8·2), anti-CD8-PerCP (SK1) and anti-CD56-PC5 (N901) (Beckman

3

Coulter). Subsequently, the cells were permeabilized, stained for intracellular IFN-γ and IL-4 using the FastImmune™ system (BD Pharmingen), resuspended in phosphate-buffered saline (PBS) containing 1% paraformaldehyde (PFA), and analysed on a flow cytometer (≈ 10 000 gated events acquired per sample).

IFN-γ enzyme-linked immunospot (ELISPOT) assay

ELISPOT assays were performed as described previously with the following modifications [28–30]. HLA-A24 restricted peptide epitopes, squamous cell carcinoma antigen recognized by T cells 2 (SART2)$_{899}$ (SYTRLFLIL), SART3$_{109}$ (VYDYNCHVDL), multi-drug resistance protein 3 (MRP3)$_{765}$ (VYSDADIFL), MRP3$_{503}$ (LYAWEPSFL), MRP3$_{692}$ (AYVPQQAWI), alpha-fetoprotein (AFP)$_{403}$ (KYIQESQAL), AFP$_{434}$ (AYTKKAPQL), AFP$_{357}$ (EYSRRHPQL), human telomerase reverse transcriptase (hTERT)$_{167}$ (AYQVCGPPL) (unpublished), hTERT$_{461}$ (VYGFVRACL) and hTERT$_{324}$ (VYAETKHFL) were used in this study. Negative controls consisted of an HIV envelope-derived peptide (HIVenv$_{584}$). Positive controls consisted of 10 ng/ml PMA (Sigma) or a CMV pp65-derived peptide (CMVpp65$_{328}$). The coloured spots were counted with a KS ELISPOT Reader (Zeiss, Tokyo, Japan). The number of specific spots was determined by subtracting the number of spots in the absence of antigen from the number of spots in its presence. Responses were considered positive if more than 10 specific spots were detected and if the number of spots in the presence of antigen was at least twofold greater than the number of spots in the absence of antigen.

Cytokine and chemokine profiling

Serum cytokine and chemokine levels were measured using the Bioplex assay (Bio-Rad, Hercules, CA, USA). Briefly, frozen serum samples were thawed at room temperature, diluted 1:4 in sample diluents, and 50 μl aliquots of diluted sample were added in duplicate to the wells of a 96-well microtitre plate containing the coated beads for a validated panel of 27 human cytokines and chemokines (cytokine 27-plex antibody bead kit) according to the manufacturer's instructions. These included IL-1β, IL-1Ra, IL-2, IL-4, IL-5, IL-6, IL-7, IL-8, IL-9, IL-10, IL-12p70, IL-13, IL-15, IL-17, basic fibroblast growth factor (FGF), eotaxin, G-CSF, GM-CSF, IFN-γ, interferon gamma-induced protein (IP)-10, monocyte chemoattractant protein (MCP)-1, MIP-1α, MIP-1β, platelet-derived growth factor (PDGF)-BB, regulated upon activation normal T cell-expressed and secreted (RANTES), TNF-α and vascular endothelial growth factor (VEGF). Eight standards (ranging from 2 to 32 000 pg/ml) were used to generate calibration curves for each cytokine. Data acquisition and analysis were performed using Bio-Plex Manager software version 4.1.1.

Arginase activity

Serum samples were tested for arginase activity by conversion of L-arginine to L-ornithine [31] using a kit supplied by the manufacturer (BioAssay Systems, Hayward, CA, USA). Briefly, sera were treated with a membrane filter (Millipore, Billerica, MA, USA) to remove urea, combined with the sample buffer in wells of a 96-well plate, and incubated at 37°C for 2 h. Subsequently, the urea reagent was added to stop the arginase reaction. The colour produced was read at 520 nm using a microtitre plate reader.

Statistical analysis

Results are expressed as means ± standard deviation (s.d.). Differences between groups were analysed for statistical significance by the Mann–Whitney U-test. Qualitative variables were compared by means of Fisher's exact test. The estimated probability of tumour recurrence-free survival was determined using the Kaplan–Meier method. The Mantel–Cox log-rank test was used to compare curves between groups. Any P-values less than 0·05 were considered statistically significant. All statistical tests were two-sided.
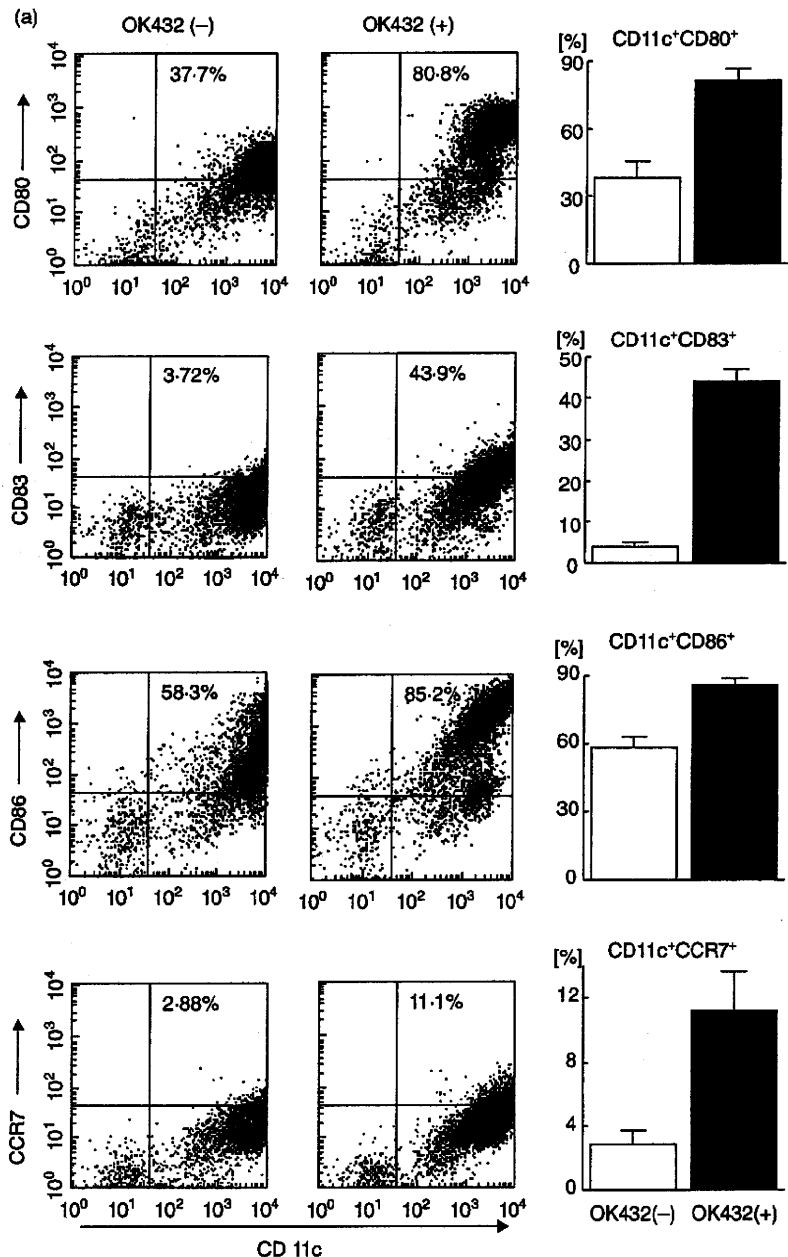
Results

Preparation of OK432-stimulated DCs

Adherent cells isolated from PBMCs of patients with cirrhosis and HCC (Table 1) were differentiated into DCs in the presence of IL-4 and GM-CSF. The cells were stimulated with 0·1 KE/ml OK432 for 3 days; 54·6 ± 9·5% (mean ± s.d.; $n = 13$) of OK432-stimulated cells showed high levels of MHC class II (HLA-DR) and the absence of lineage markers including CD3, CD14, CD16, CD19, CD20 and CD56, in which 30·9 ± 14·2% were CD11c-positive (myeloid DC subset) and 14·8 ± 11·2 were CD123-positive (plasmacytoid DC subset), consistent with our previous observations [20]. As reported [32,33], greater proportions of the cells developed high levels of expression of the co-stimulatory molecules B7-1 (CD80) and B7-2 (CD86) and an activation marker (CD83) compared to DCs prepared without OK432 stimulation (Fig. 1a). Furthermore, the chemokine receptor CCR7 which leads to homing to lymph nodes [13,34] was also induced following OK432 stimulation.

To evaluate the endocytic and phagocytic ability of the OK432-stimulated cells, uptake of FITC-dextran was quantitated by flow cytometry (Fig. 1b). The cells showed lower levels of uptake due to maturation compared to DCs prepared without OK432 stimulation, while the OK432-stimulated cells derived from HCC patients preserved a moderate uptake capacity. As expected, the OK432-stimulated cells produced large amounts of cytokines IL-12 and IFN-γ (Fig. 1c). In addition, they displayed high cyto-

Fig. 1. Effects of OK432 stimulation on the properties of dendritic cells (DCs) generated from blood monocyte precursors in patients with cirrhosis and hepatocellular carcinoma (HCC) ($n = 13$). (a) Lineage cocktail 1 (lin 1⁻) human leucocyte antigen D-related (HLA-DR⁻) subsets with [OK432(⁺)] and without [OK432(⁻)] stimulation were analysed for surface expression of CD80, CD83, CD86 and CCR7. Dot plots of a representative case are shown in the left-hand panel. Mean percentages [±standard deviation (s.d.)] of positive cells are indicated in the right-hand panel. OK432 stimulation resulted in the expression of high levels of CD80, CD83, CD86 and CCR7 in the lin 1⁻human leucocyte antigen D-related (HLA-DR⁻) DC subset. (b) DC subsets with and without OK432 stimulation were incubated with fluorescein isothiocyanate (FITC) dextran for 30 min and the uptake was determined by flow cytometry. A representative analysis is shown in the upper panel. Mean fluorescence intensities (MFIs) (±s.d.) of the positive cells are indicated in the lower panel. OK432-stimulated cells showed lower levels of uptake due to maturation. (c) DC supernatants were harvested and the concentrations of interleukin (IL)-12 and interferon (IFN)-γ measured by enzyme-linked immunosorbent assay (ELISA). OK432-stimulated cells produced large amounts of the cytokines. The data indicate means ± s.d. of the groups with and without the stimulation. All comparisons in (a–c) [OK432(+) *versus* OK432(⁻)] were statistically significant by the Mann-Whitney U-test ($P < 0.005$). (d) Tumoricidal activity of DCs assessed by incubation with ⁵¹Cr-labelled Hep3B, PLC/PRF/5 and T2 targets for 8 h at the indicated effector/target (E/T) cell ratios. OK432-stimulated cells displayed high cytotoxic activity against the target cells. The results are representative of the cases studied.

toxic activity against HCC cell lines (Hep3B and PLC/PRF/5) and a lymphoblastoid cell line (T2) although DCs without OK432 stimulation lysed none of the target cells to any great degree (Fig. 1d). Taken together, these results demonstrate that OK432 stimulation of IL-4 and GM-CSF-induced immature DCs derived from HCC patients promoted their maturation towards cells with activated phenotypes, high expression of a homing receptor, fairly well-preserved phagocytic capacity, greatly enhanced cytokine production and effective tumoricidal activity, consistent with previous observations [16,19].

Safety of OK432-stimulated DC administration

Prior to the administration of OK432-stimulated DCs to patients, the cells were confirmed to be safe in athymic nude mice to which 100-fold cell numbers/weight were injected subcutaneously (data not shown). Subsequently, OK432-stimulated DC administration was performed during TAE therapy in humans, in which DCs were mixed together with absorbable gelatin sponge (Gelfoam) and infused through an arterial catheter following iodized oil (Lipiodol) injection, as reported previously [20]. Adverse events were

5